Article:
AL-Jarazi, R., Rahman, A. orcid.org/0000-0003-3076-7942, Ai, C. et al. (2 more authors) (2024) Evaluation and prediction of interface fatigue performance between asphalt pavement layers: application of supervised machine learning techniques. International Journal of Pavement Engineering, 25 (1). 2370551. ISSN 1029-8436

https://doi.org/10.1080/10298436.2024.2370551

Evaluation and prediction of interface fatigue performance between asphalt pavement layers: application of supervised machine learning techniques

Rabea AL-Jarazi[a,b], Ali Rahman[a,b,c*], Changfa Ai[a,b], Chaoyang Li[a,b], and Zaid Al-Huda[d]

rabeacivil@my.swjtu.edu.cn; arahman@swjtu.edu.cn; cfai@swjtu.edu.cn; 2924603656@my.swjtu.edu.cn; eng.zaidalhuda@gmail.com.

[a]*School of Civil Engineering, Southwest Jiaotong University, Chengdu Sichuan 610031, China.*

[b]*Key Laboratory for Highway Engineering of Sichuan Province, Southwest Jiaotong University, Chengdu, Sichuan 610031, China.*

[c] *School of Civil Engineering, Faculty of Engineering and Physical Sciences, University of Leeds, Leeds, UK*

[d]*Department of Computing and Artificial Intelligence, Southwest Jiaotong University, Chengdu, Sichuan 610031, China.*

*Corresponding author: E-mail address: arahman@swjtu.edu.cn (Ali Rahman)

Address: School of Civil Engineering, Southwest Jiaotong University, No. 111, 1st Northern Section, Second Ring Road, Chengdu, Sichuan 610031, China. Mobile:(+86)158-8455-1418

Evaluation and prediction of interface fatigue performance between asphalt pavement layers: application of supervised machine learning techniques

Abstract:

Assessing interlayer fatigue performance is key to ensuring the durability and structural integrity of asphalt pavements. This research pioneers the application of supervised machine learning (ML) techniques in estimating interface fatigue life (IFL) and interface shear stiffness (ISS) between asphalt layers. Utilizing 84 lab-prepared specimens, tested under diverse conditions—temperature, normal pressure, loading frequency, and shear stress, with a constant tack coat type and application rate—enabled the training and validation of predictive models. Based on the experimental results, the study evaluated the influence of each factor on fatigue indices before employing genetic expression programming (GEP) and artificial neural networks (ANNs) for prediction. The efficacy of these models was quantified using several statistical metrics, highlighting their robustness in predicting IFL and ISS. A comparative analysis showed the ANN model's superior performance (R^2=0.980, RMSE=0.826, MAE=0.636 for ISS and R^2= 0.972, RMSE=0.498, MAE=0.383 for IFL) over the GEP model (R^2=0.921, RMSE=1.402, MAE=1.079 for ISS and R^2=0.913, RMSE=0.623, MAE=0.479 for IFL). Sensitivity analysis confirmed the models' alignment with experimental data. Finally, the analysis of importance of variables revealed temperature as the most critical and frequency as the least influential factor on interface fatigue performance. The findings of this study could further pave the way for the realization of a reliable and efficient design of interlayer bonding between asphalt pavement layers.

Keywords: Asphalt pavement, interface fatigue life, interface shear stiffness, machine learning, genetic expression programming, artificial neural networks

1. Introduction

In recent years, the durability of asphalt pavement structures has become increasingly critical owing to the rapid growth in traffic volumes, vehicle loads, and the effect of more severe than before climatic

conditions. As a result, there is a greater demand for enhanced performance standards. Asphalt pavement, commonly referred to as flexible pavement, is a multi-layered structure consisting of various materials, with each layer playing a distinct role. It is widely recognized that the durability of the pavement structure is affected not only by the overall design, properties of the materials used, and construction quality but also by the bonding condition at the layer interface between the adjacent layers.

Layer interface between successive layers in a pavement structure experiences both shear and normal stresses simultaneously and repeatedly during its service life. As a result, the interface stiffness will be negatively influenced due to the cyclic loading, leading to a reduction in interface fatigue life. The sufficient bond at layer interface allows continuous distribution of stresses within the pavement structure and reduces the damage and cracks between pavement layers. In practice, insufficient bonding may prematurely cause several distresses and performance degradation as the debonded structure no longer behaves as a monolithic structure. Consequently, it can significantly impact the pavement's durability and longevity during its service life (Uzan J et al. 1978, Romanoschi and Metcalf 2001, Tashman et al. 2006, Alae et al. 2020, Mohammad et al. 2009, Salinas et al. 2013). In this context, many studies have addressed this issue. Khweir and Fordyce (2003) reported that interface bonding failure between surface course and binder course could lead to a predicted loss of 40% of the potential life of a pavement. Similarly, West et al. (2005) reported that with only a 10% loss of bond strength, a 50% reduction in fatigue life could be expected. Moreover, a study conducted by Roffe and Chaignon (2002) revealed that the absence of bonding between successive layers in a pavement would result in a considerable 60% decrease in its overall longevity. Furthermore, these issues increase maintenance costs and negatively influence pavement durability (Vaitkus et al. 2011).

The reasons behind poor bonding have not been fully understood thus far, but certain contributing factors seem to play a significant role in causing debonding between the layers of pavement. These factors include mixture properties (air voids, type of aggregate, materials content), structural parameters (layer thickness, tack coat type, dosage), surface characteristics (roughness, cleanness, durst), construction parameters (compaction, temperature, aging, contamination), and environmental conditions (high and low

temperature, freeze and thaw cycle, frost, moisture) (Mohammad et al. 2002, Partl et al. 2008, Leng et al. 2009, Raab et al. 2009, Hun et al. 2012, Raposeiras et al. 2013, Salinas et al. 2013, Johnson et al. 2015). Figure 1 presents a comparison of the stress distribution for two different bonding conditions in an asphalt pavement under traffic loading.

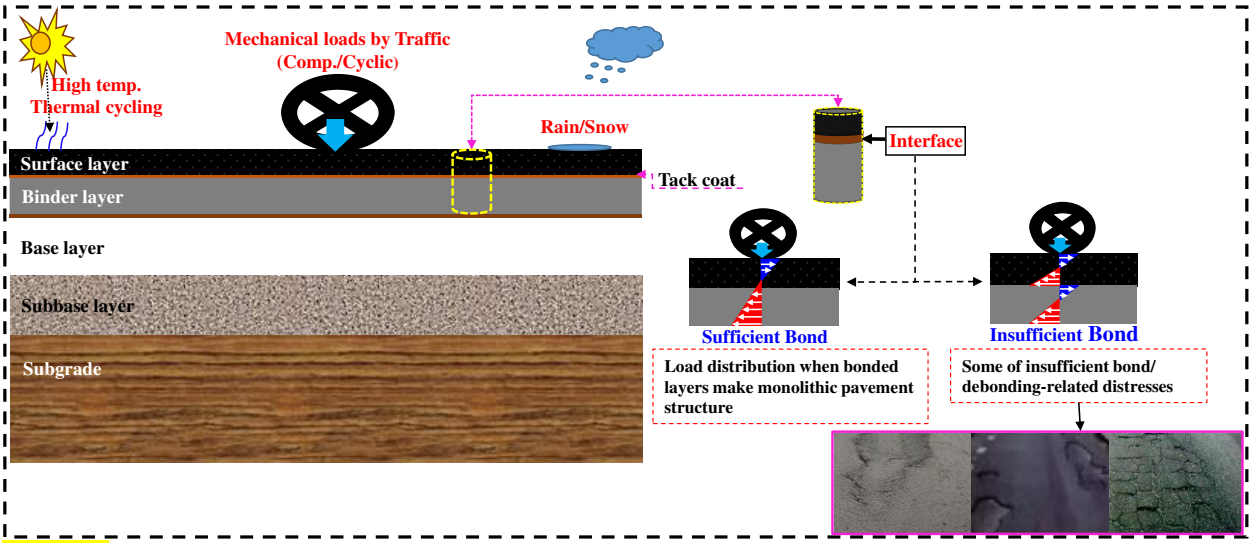

Figure 1. Stress distribution between adjacent layers of an asphalt pavement with two different bonding conditions.

Given this background, it can be realized that the evaluation and accurate prediction of interlayer performance between adjacent asphalt layers is crucial for ensuring the longevity and structural integrity of the pavement structure. Interface bonding properties in asphalt pavement are mostly evaluated using monotonic and cyclic loading tests. Rahman et al. (2017) classified test methods for evaluating interface bonding into eleven distinct test protocols. Among which, the monotonic direct shear test is the most widely used method to evaluate the interface bonding strength. However, the monotonic behavior is not representative of typical in-situ traffic loading conditions (which are cyclic in nature). Cyclic loading tests are employed to assess fatigue properties of interface bonding. These tests measure the interface stiffness at small strain amplitudes and evaluate the resistance to repeated shear loads, including fatigue life and permanent strain accumulation. As such, cycle tests provide valuable insights into the interface's damage behavior over the pavement's lifespan, which can be beneficial for pavement design and modeling purposes. Researchers have developed numerous test methods to study the fatigue behaviour of interface

bonding between asphalt pavement layers. These methods include an inclined testing configuration (Romanoschi and Metcalf 2001), a customized double shear testing (DST) device (Diakhaté et al. 2011), a repeated direct shear box test (Tozzo, Fiore, et al. 2014), a direct shear fatigue test (Song et al. 2016), a four-point shear setup (Rahman et al. 2019), and a shear-torque fatigue testing (Ragni et al. 2020) to analyze and investigate the interlayer fatigue performance of double-layered asphalt specimens.

Moreover, various studies have implemented numerical analysis methods to investigate and analyze the fatigue behavior of interlayer bonding. Cho et al. (2019), for instance, utilized the FlexPAVE simulation software to study how debonded pavement structures influence fatigue cracking. Using the same software and informed by cyclic shear test data, Ragni et al (2022) developed a three-dimensional (3D) finite element model to measure bond properties at the interface. In a related effort, Yao et al (2024) developed a numerical model with the EverStressFE program, aiming to analyze the responses of asphalt pavement under various interlayer bonding conditions. The behavior of asphalt pavement interlayers, subjected to diverse loading and temperature conditions, has been thoroughly investigated and assessed using ABAQUS software (Guo et al. 2016, Rahman et al. 2021 , and Kim et al. 2011).

Although these approaches provide reliable results, they often involve high costs and time-consuming processes. Furthermore, complex loading conditions and stress state at layer interface, compounded by a combination of a number of factors, such as temperature, humidity, and other environmental circumstances, result in complex and nonlinear behavior of the interface.

To address the aforementioned challenges, recent advances in soft computing and data science resulted in a rapid development of artificial intelligence (AI) and machine learning (ML) as promising alternative techniques owing to their competence in solving complex problems. In this context, different studies were conducted, focusing on calibrating ML algorithms to generate models that describe the behavior of interlayers. These models aim to capture the response of the interface under different influencing parameters within a given range. Table 1 summarizes these works and the developed models related to interface bonding characteristics between asphalt pavement layers. The table reveals that the application of ML models has a superior capability to predict and explain the experimental data with high accuracy

and low computational cost. Furthermore, it is found that the most frequently used ML technique is artificial neural networks (ANNs).

Table 1: Developed ML models related to interface bonding characteristics between asphalt pavement layers.

Year	Outputs	Test conditions and input variables	Model	Findings	Authors
2013	Interlayer shear bond properties	• Static test. • Temperature: 20 and 40°C • Traffic loading: ADT (9800 to 94990vpd) and percentage of heavy vehicles (2.6 to 11.1t) • Aggregate passing through sieve 8, 2, and 0. 09 mm (layer 1) • Aggregate passing through sieve 8, and 2 mm (layer 2) • Void content of layer 1: 4 to 12.8% • Void content of layer 2: 4.4 to 9.9% • Age: aged and non-aged	Artificial Neural Networks	Artificial Neural Network are suitable for deriving models from datasets and to predict interlayer shear bond properties	Raab et al. (2013)
2015	Interlayer bond strength	• Static test. • Type of tack coat: Cationic emulsion (200g/m^2), SBS polymer -modified tack coat (300g/m^2) and no tack coat • Age: aged and non-aged • Void content of layer 1: 4 to 12.8% • Void content of layer 2: 4.4 to 9.9% • Temperature 10 to 35°C • Deformation rate: 0.5 to 9.5 mm/min	Artificial Neural Networks	Artificial Neural Networks can model data and predict interlayer bond strength	Raab et al. (2015)
2022	Interlayer shear strength	• Static test. • Aggregate diameter: 12.5mm (AC12.5), 19mm (AC19), and 25 mm (AC25) • Tack coat type: Emulsion CRS-1 • Tack coat application rate: 0.5 l/m^2 • Temperature: 25, 40 and 60°C. • Normal pressure: 0, 0.14, 0.2, 0.4, and 0.6 MPa.	Adaptive Neuro Fuzzy Inference System with metaheuristic optimization Algorithms	High accuracy of prediction $R^2 = 0.95$	Dao et al. (2022)
2022	Interlayer shear strength	• Static test. • Specimen composition: AC-13/ AC-20, AC-16/ AC-20 and AC-13/ AC-16;	Artificial Neural Networks	High accuracy of prediction $R^2 = 0.99$	Nian et al. (2022)

		• Tack coat type: Base asphalt, SBS-modified asphalt, emulsified asphalt, and no tack coat; • Tack coat dosage: 0.16 –0.66 l/m^2 • Shear angle: 15, 40, 60, and 90° • Temperature: -20, 0, 20, 45, and 58°C • Loading rate: 3, 8, 16, 30, 40, and 50 mm/min			
2023	Interlayer shear strength	• Static test. • Specimen composition: AC-11/ AC-16 • Temperature: 0, 10, 20, 30, and 40°C • Normal stress: 0 to 0.6MPa • Tack coat type: Conventional Emulsion, Modified Emulsion and no tack coat • Curing-time: Short and Medium • Shear deformation rate: 0.5 to 9.5mm/min • Layer thickness of top and bottom layers • Air void content of top and bottom layers • Asphalt content of top and bottom layers • Tack coat application rate: 0.0, 0.15, and 0.3 kg/m^2	Random forest and Feed-Forward Artificial Neural Networks	High accuracy of prediction $R^2 = 0.96$	Al-Jarazi et al. (2023)
2024	Interface bonding strength	• Static test. • Specimen composition: AC-13/ AC-20 • Temperature: 5, 20, 35, and 50°C • Shear stress: 0, 0.05, 0.1, 0.15, and 0.20MPa • Tack coat type: Cationic emulsified asphalt • Tack coat application rate: 0.4 to 1.6 kg/m^2	Feed-Forward Backpropagation Artificial Neural Networks	High accuracy of prediction $R^2 = 0.99$	Al-Jarazi et al. (2024)

It can be seen that existing models currently available are trained to predict the behavior of interface bonding under a monotonic loading condition. However, thus far, there have been no specific developments of ML models to predict the interface fatigue behavior, considering a comprehensive range of parameters and properties. It is noteworthy that accurate prediction and evaluation of interlayer fatigue

performance is of great importance to the overall performance of the pavement structure. In this regard, Interface fatigue life (IFL) and interface shear stiffness (ISS) are two common evaluation indexes of the interface fatigue performance.

All things considered, this study aims to employ two ML-based techniques namely, gene expression programming (GEP) and artificial neural networks (ANNs) for the accurate estimation of IFL and ISS in asphalt pavement from limited input-determined parameters. Variables of test temperature, normal pressure, loading frequency, and shear stress were selected to conduct laboratory experiments on double-layered asphalt beam specimens made up of stone mastic asphalt (SMA-13) and asphalt concrete (AC-20). The ANN and GEP algorithms were employed due to their effectiveness in solving complex problems. Such models can provide time and cost-saving options for the purposes of initial design, construction, and maintenance of asphalt pavement. ANN is commonly used to address complex nonlinearities between predictors and responses as mentioned in Table 1. On the other hand, the GEP technique has demonstrated a high potential for using mathematical functions to solve complex problems and provide accurate predictions (Ashteyat et al. 2020). For example, Liu et al. (2017) employed the GEP algorithm to develop a predictive model of the dynamic modulus of asphalt mixtures. In another study, multigene genetic programming (MGGP) was used to predict asphalt concrete fatigue performance subjected to the 3-point bending cylinder fatigue test (Seitllari and Kutay 2023). The developed models based on GEP algorithm exhibited improved prediction accuracy compared to the regression-based models. The GEP technique utilizes a diverse range of inputs to construct an optimal model. By minimizing errors and ensuring robust fitness, it achieves accurate predictions of outcomes. In this study, the universality of the developed models was further tested to provide a theoretical basis for reviewing the parameters that influence the interlayer fatigue behavior of asphalt pavement. This step was taken to validate the reliability of the proposed models.

The structure of this article is as follows. In Section 2, the methodology adopted in this study was introduced, including the experimental program and the proposed ML techniques. Section 3 introduces performance measures, discussing the various indices critical for evaluating the accuracy, reliability, and

precision of the developed models. Section 4 presents the results and discussion, including experimental findings, the application of proposed ML (ANN and GEP) models, comparisons of model performance, and a sensitivity analysis to further validate the universality of the prediction models. Finally, Section 5 concludes the paper, summarizing the key findings and contributions.

2. Methodology

This research work was carried out in two phases. The first phase involved laboratory experiments to evaluate the interlayer fatigue performance. During this stage, composite asphalt beam specimens, consisting of SMA and AC mixtures, were designed and produced. The tests were carried out with a developed 4-point shear setup which can also apply normal pressure perpendicular to the interface plane. The test factors considered in this study are temperature, normal stress, loading frequency, and shear stress. The material used as tack coat is a high-performance styrene butadiene styrene (SBS)-modified asphalt binder. The effect of each parameter on the ISS and IFL were evaluated. In the subsequent phase, data from the initial laboratory experiments were processed and utilized in this phase, where ANN and GEP techniques were developed for forecasting and evaluating the interlayer fatigue indices. Figure 2 illustrates an overview of the methodology introduced in this study.

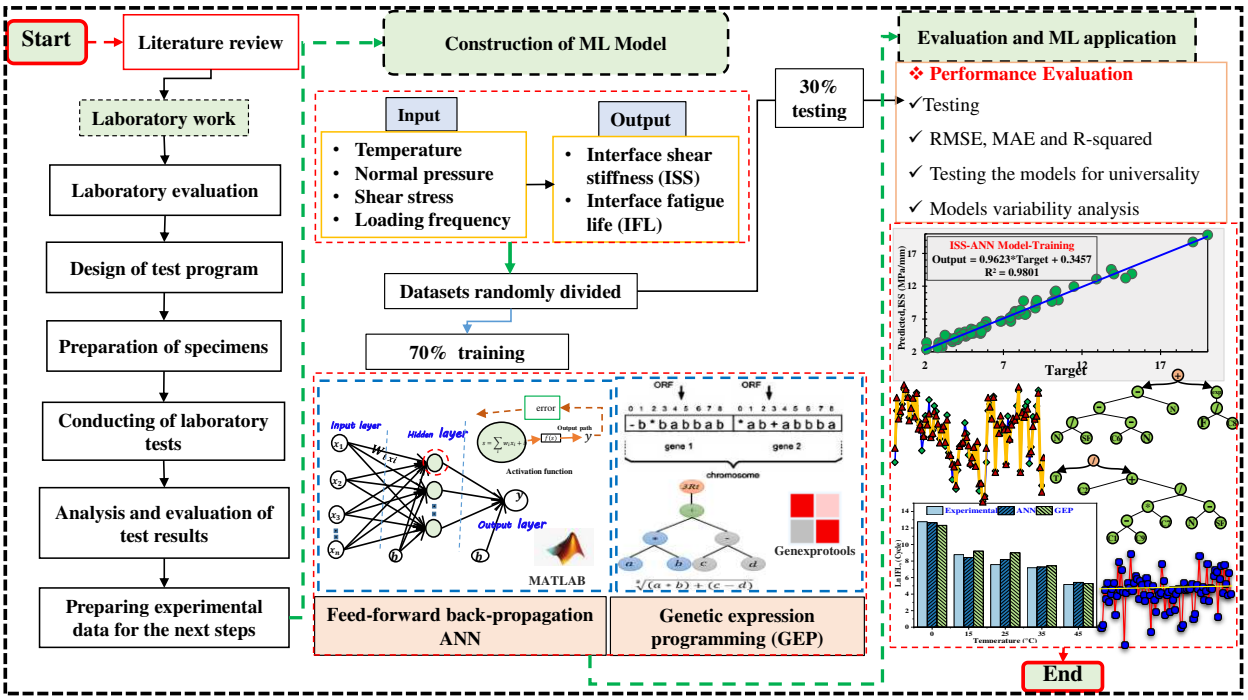

Figure 2. An overview of the proposed approach in this study.

2.1. Experimental program

2.1.1. Materials

Interface shear fatigue assessment was performed through a four-point shear setup installed in an environmental chamber of a universal testing machine (UTM). The tests were carried out with a total number of 84 double-layered asphalt beam specimens, comprising of stone mastic asphalt (SMA-13) and asphalt concrete (AC-20). Table 1 displays the aggregate gradation design of two mixtures as per the Chinese Specification for Highway Asphalt Pavement Construction (JTGF40-2004 (Code of China 2004)). Limestone was utilized for both coarse and fine aggregates in the preparation of asphalt mixtures. These aggregates were clean, dry, free of weathered particles, and pure. Mineral limestone powder was used as filler. Properties of mineral materials were met the specification requirements (JTG F40-2004 (Code of China 2004)). Two mixtures were prepared using an SBS-modified asphalt binder with properties shown in Table 2. The optimum asphalt content of SMA-13 and AC-20 mixtures by percentage of weight was 5.8% and 4.5%, respectively. The tack coat material utilized at layer interface was a high-performance SBS-modified emulsified asphalt. Properties of tack coat material are presented in Table 3.

Table 1. Aggregate gradation of mixtures.

Mixture Type	Sieve size (mm)											
	26.5	19	16	13.5	9.5	4.75	2.36	1.18	0.6	0.3	0.15	0.075
	Passing percentage (%)											
SMA-13	100	100	100	95	62.5	27	20.5	19	16	13	12	10
AC-20	100	95	85	71	61	41	30	22.5	16	11	8.5	5

Table 2. Properties of the SBS modified asphalt.

Property	Unit	Test result	Specification limit
Penetration (100 g, 5 s, 25°C)	0.1mm	41.1	≥ 40
Ductility at 15°C	cm	75	≥ 50
Softening point (R & B)	°C	112.1	≥ 85
Flashpoint	°C	276	≥ 260
Tests on residue after rolling thin-film oven (RTFO) test			
Mass loss	%	0.06	≤ 0.6
Penetration ratio	%	88.2	≥ 65

Table 3. Properties of tack coat material.

Property	Unit	Test result	Specification limit
Softening point (R & B)	°C	113.4	≥ 85
Penetration (100 g, 5 s, 25°C)	0.1mm	42.8	≥ 40
Ductility at 15°C	cm	68	≥ 50
Flexural tensile toughness (-20°C)	kPa	427.5	≥ 400
Flexural tensile modulus (-20°C)	MPa	96.5	≤ 100
Tests on residue after rolling thin-film oven test			
Mass loss	%	0.002	≤ 0.6
Penetration ratio	%	83.1	≥ 65

Flash point	°C	265	≥ 260

2.1.2. Specimen preparation

In this study, rectangular beams with two halves representing a double-layered asphalt mixture and a vertical interface plane in between for tack coat application were manufactured. To produce asphalt beam specimens, a steel mold with the plan dimensions 300mm × 400mm and 100mm depth was used in this experiment. In addition, a removable vertical steel plate was installed in the middle of the steel mold to divide the mold in two halves for mixture preparation. The specific specimen preparation process is as follows:

1) An adequate amount of the loose AC-20 asphalt mixture was poured into one-half of the mold, and then it was evenly distributed. Afterward, a roller compactor was utilized to compact the mixture to its maximum density with a 5% air void content and the desirable thickness of 100 mm. The compacted mixture was then allowed to cool down to room temperature for 1 day before tack coat application.
2) In the second stage, the movable steel plate was removed, and the tack coat material was uniformly sprayed on the cleaned surface at desired application rate (0.30 L/m^2) accordingly. Subsequently, the coated surface was set aside at room temperature for 2 hours to allow the curing procedure to be completed.
3) Following the application of the tack coat and its curing, the loose SMA mixture (160℃) was placed into the second half of the mold and compacted using a similar method applied in the first half of the mold. The target air void content of the SMA-13 mixture was set at 3.5%. Before performing the cutting operation, the slab was allowed to cool and cure at room temperature for one day, and the mold was detached form the prepared slab accordingly.

4) Finally, each slab was marked to match the final specimen's dimensions. The extra parts from each side were sawed, and five test specimens were obtained from the slab's remaining part.

Figure 3 illustrates the laboratory procedure for fabricating specimens to conduct interface shear fatigue tests.

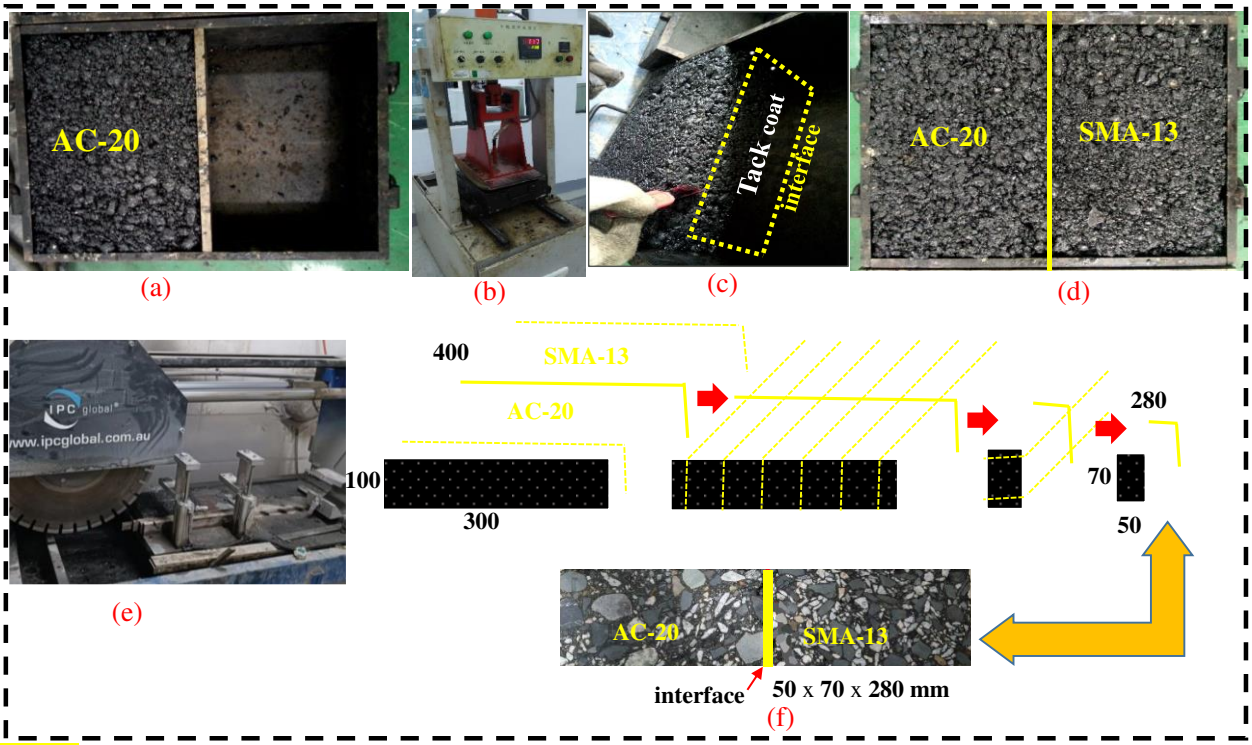

Figure 3. Laboratory procedure for fabricating specimens: (a) Placing AC-20 mix, (b) Mix compaction, (c) Application of tack coat, (d) Laying SMA-13 mix, (e) Specimen cutting, and (f) Final specimen.

The unusual compaction method for specimen preparation used in this study differs from the compaction methods commonly employed for lab-scale interface bonding investigations. As such, the lack of vertical compaction between layers represents a limitation of the current experimental methodology. However, roller compaction was selected to improve simulation of realistic field construction conditions and air void distributions within each independent asphalt layer. Future studies will explore specimen fabrication methods that balance both constructability and representation of field bonding.

2.1.3. Four-point shear device

In this study, a new four-point shear device was developed to assess interface shear bonding, as illustrated in Figure (4). This apparatus represents an advancement over the original device (De Bondt 1999), featuring modifications in the force distance and orientation of the central two points, allowing the loading block to exert shear stress parallel to the interface plane. A cylinder-pump assembly was also integrated to apply normal stress perpendicular to the interface plane. The vertical shearing load, which simulates the shear forces acting on pavement surface as a result of vehicle maneuvering, was generated by the actuator of the universal testing machine (UTM-100).

The double-layered asphalt specimen (280 × 70 × 50 mm) was positioned within the clamps ensuring the interface lay within the two central clamps (the interface zone), with a center-to-center distance of 60 mm between them. This setup is designed to induce interface failure in this zone through shear stress from the repeated loading by the UTM actuator. The device for applying the normal pressure, representing the wheel load on roads, delivers controllable and consistent pressure. The normal load feature consists of a cylinder, a hose, a pump, a load measurement system, and load distribution plates. Upon specimen placement within the clamps, load distribution plates are affixed to each end. Subsequently, hydraulic pump pressure is applied to the cylinder until it extends to the distribution plate. The applied normal load on the specimen is continuously monitored by a load cell located on the opposite side. To gauge relative vertical shear displacement at the interface, two linear variable differential transducers (LVDTs) were attached to the interface zone of the specimen. Data from the load cell, confining pressure transducer, and LVDTs were gathered using a data acquisition system. The entire setup was housed within the UTM's environmental chamber, enabling testing at temperatures ranging from -40°C to 100°C, as shown in Figure 4(b). This setup allows for observing of the evolution of applied shear force and relative displacement during fatigue tests. Fifty data points per loading/displacement cycle were used for detailed plotting. In this study, the traditional 50% stiffness reduction threshold was used to determine the

interface shear fatigue life. Fatigue life is defined as the number of loading cycles correspond to 50% reduction in initial shear stiffness modulus.

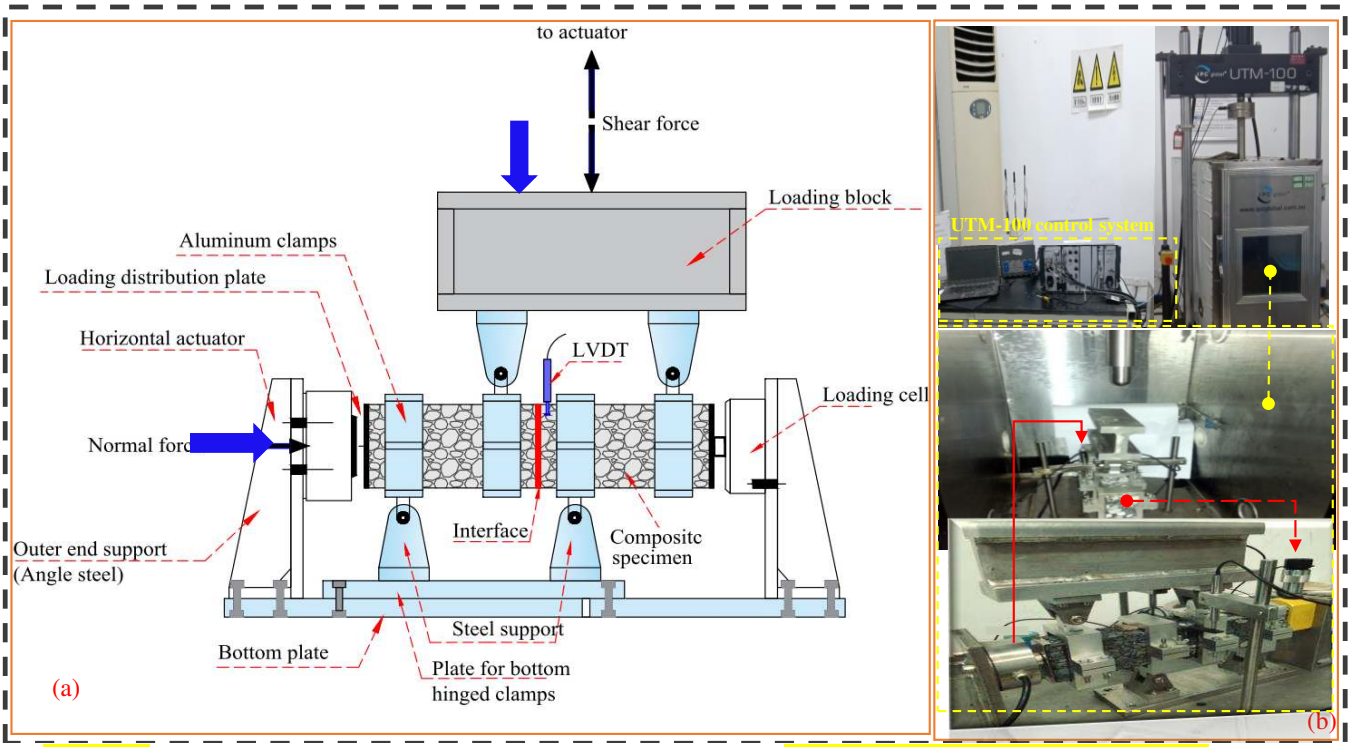

Figure 4. Four-point shear test device: (a) schematic diagram; (b) The whole set up inside the UTM.

2.1.4. Experimental design

In the experimental design, a range of variables including temperatures, loading frequencies, shear stress amplitudes, and normal pressure levels were selected to assess and analyze the interface shear fatigue behavior, specifically focusing on interface shear stiffness (ISS) and interface fatigue life (IFL).

During the fatigue testing, the shear stress amplitude ranged from 30% to 50% of the interface shear strength, as determined through monotonic shear testing. This testing was performed at a loading rate of 2.54 mm/min, under conditions of zero normal stress. Six distinct shear stress levels—163, 180, 196, 212, 294, and 359 kPa—were carefully selected. Correspondingly, six levels of normal load—0, 10, 20, 35, 45, and 55 kN, equivalent to compressive stress levels of 0, 28, 56, 98, 126, and 154 kPa—were chosen. This selection was chosen based on a previous study (D'Andrea and Tozzo 2016) and taking into account the dimensions of the specimen.

To evaluate the influence of temperature on interlayer shear fatigue, this study considered different temperature levels as -10, 0, 15, 25, 35, and 45 °C. In addition, five load frequency levels of 1, 4, 5, 8, and 10 Hz were selected to represent the driving speeds of 4, 17, 21, 35, and 45km/h. To better simulate the cyclic nature of traffic loading, the tests were carried out under force-controlled mode with a continuous haversine waveform. While a contact load of 0.1kN was chosen and maintained during the testing process, the desired shear load was applied to the specimen to induce shear fatigue failure.

To conclude, Table 4 summarizes the experimental parameters, which are utilized as input variables in the proposed prediction models, along with their specific levels. These parameters and their corresponding ranges were carefully selected to effectively mimic a range of field conditions.

Table 4 Test factorial for prepared specimens.

Parameter Settings	Variables	Levels
Influential factors	Normal stress (kPa)	0, 28, 56, 98, 126, 54
	Frequency (Hz)	1, 4, 5, 8, 10
	Temperature(°C)	-10, 0, 15, 25, 35, 45
	Shear stress	163, 180, 196, 212, 294, 359

2.2. Supervised machine learning techniques

2.2.1. Artificial neural networks (ANNs)

ANNs are supervised machine learning algorithms that are inspired by the neural architecture of the human brain, reflecting its extensive connectivity and ability to learn from inputs. Multi-layer forward feedback propagation ANN is one of the most popular algorithms that learns and improves processes by examining input data to produce accurate predictions (Ozturk and Kutay 2014) . It consists of interconnected artificial neurons or processing elements organized in layers. The layers include the input layer, representing an input vector; the output layer, responsible for generating the output; and the hidden

layers situated between them. The hidden layers constitute the majority of the ANN structure, and each hidden layer consists of a set of neurons, as illustrated in Figure 5. In this algorithm, the inputs are multiplied by the weights of the links connecting the inputs and the hidden neurons. Next, the sum of previous values will pass through the activation function which will produce a value that is the input to the next layer. The output of any given layer will become the input of the next layer. This process is called feed forward. The relationship between inputs and outputs is expressed in Equation (1).

$$Y = f(s) = f(b + \sum_{i=1}^{n} w_i x_i) \quad (1)$$

where x_i refers to the input, w_i refers to the weight, and b is the bias at each neuron.

The difference between the target value and the network output is measured as the error. To improve the network performance, a training algorithm called Levenberg-Marquardt training backpropagation algorithm was utilized in this study. This algorithm facilitates the adjustment of connection weights within the network, starting at the output layer and progressing towards the input layer, by propagating the error backwards. This iterative process of forwarding and back-correcting (updating) of link weights continues until a satisfactory level of performance is achieved, indicating the completion of the training phase. Thus, the network uses the final weights obtained through training to make predictions (Basheer and Hajmeer 2000).

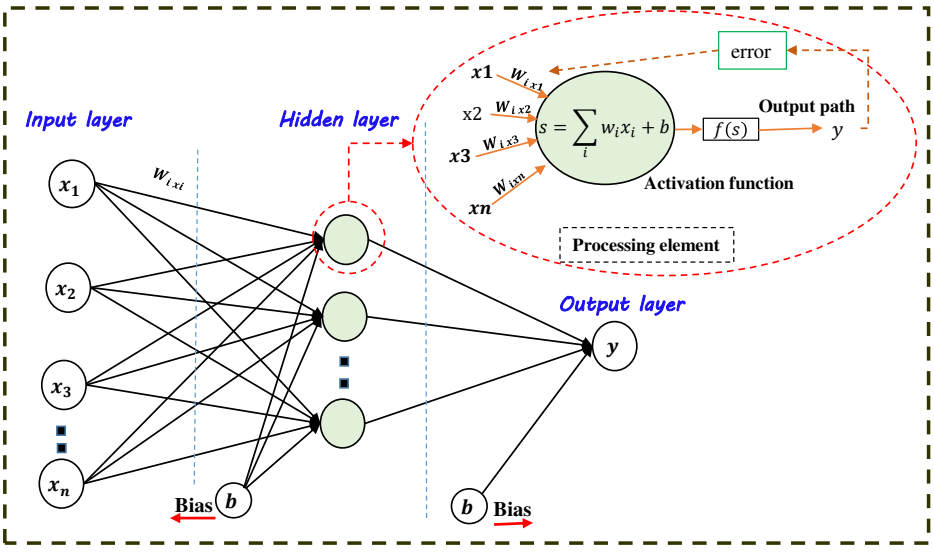

306 Figure 5. Schematic structure for ANN algorithm.

307 *2.2.2. Gene expression programming (GEP)*

308 GEP, developed by Ferreira (Ferreira 2001), is one of the most effective supervised machine learning-
309 based prediction and estimation techniques. The basic principles of the GEP as a branch of genetic
310 programming (GP), are based on the law of evolution from Darwin's theory of evolution and Mendel's
311 genetic theory (Gao 2018). It consists of five main components: (1) function set, (2) terminal set, (3)
312 fitness function, (4) control parameters, and (5) stop condition. In this study, a fixed-length character
313 string approach was adopted to obtain solutions within the GEP algorithm. This stands in contrast to
314 conventional GP, where a parse-tree representation is employed, and its length can dynamically vary
315 during the program's execution. A computer model of these solutions is presented in the form of
316 expression trees (ETs). In the GEP algorithm, the creation of the genetic variety is highly simplified
317 because genetic operators work at the chromosome level. Moreover, GEP's multi-genic structure
318 empowers it to develop complex, nonlinear programs composed of multiple subprograms.
319 Each GEP gene comprises a fixed-length list of symbols, with each symbol drawn from a defined set of
320 functions or terminals. In other words, each gene consists of two components: the head part, which
321 encompasses both terminals such as (i, j, 3, 5) and functions like (+, -, / , *), and the tail, which only
322 contains terminals.
323 The GEP algorithm encodes the essential information for developing empirical relationships within
324 chromosomes and employs the Karva language to facilitate this process (Kara 2013, Gandomi and Roke
325 2015). Karva expression (K expression) allows both genotype and phenotype to be inferred from gene
326 sequences. These genotypes and phenotypes are encoded separately in GEP. (see Figure 6 (a and b)). The
327 transformation from Karva to ET begins at the leading ET position and proceeds along the string.
328 Conversely, ETs can be converted into K expression by recording nodes from the root layer to the deepest
329 layer. The size of ETs varies in the GEP algorithm, resulting in a certain number of redundant elements
330 that are not utilized for genome mapping. Thus, GEP gene lengths and K expression may differ.

Figure 6(c) illustrates the base structure of GEP algorithm, starting with the random creation of fixed-length chromosomes for individuals. These chromosomes are then evaluated for fitness, and individuals are selected for reproduction based on their fitness scores. This selection process serves as the foundation for the subsequent application of genetic operations. The cycle iterates over multiple generations with newly generated individuals until a viable solution is achieved. In this technique, genetic operations, including mutation, rotation, and crossover are conducted to facilitate conversions within the population.

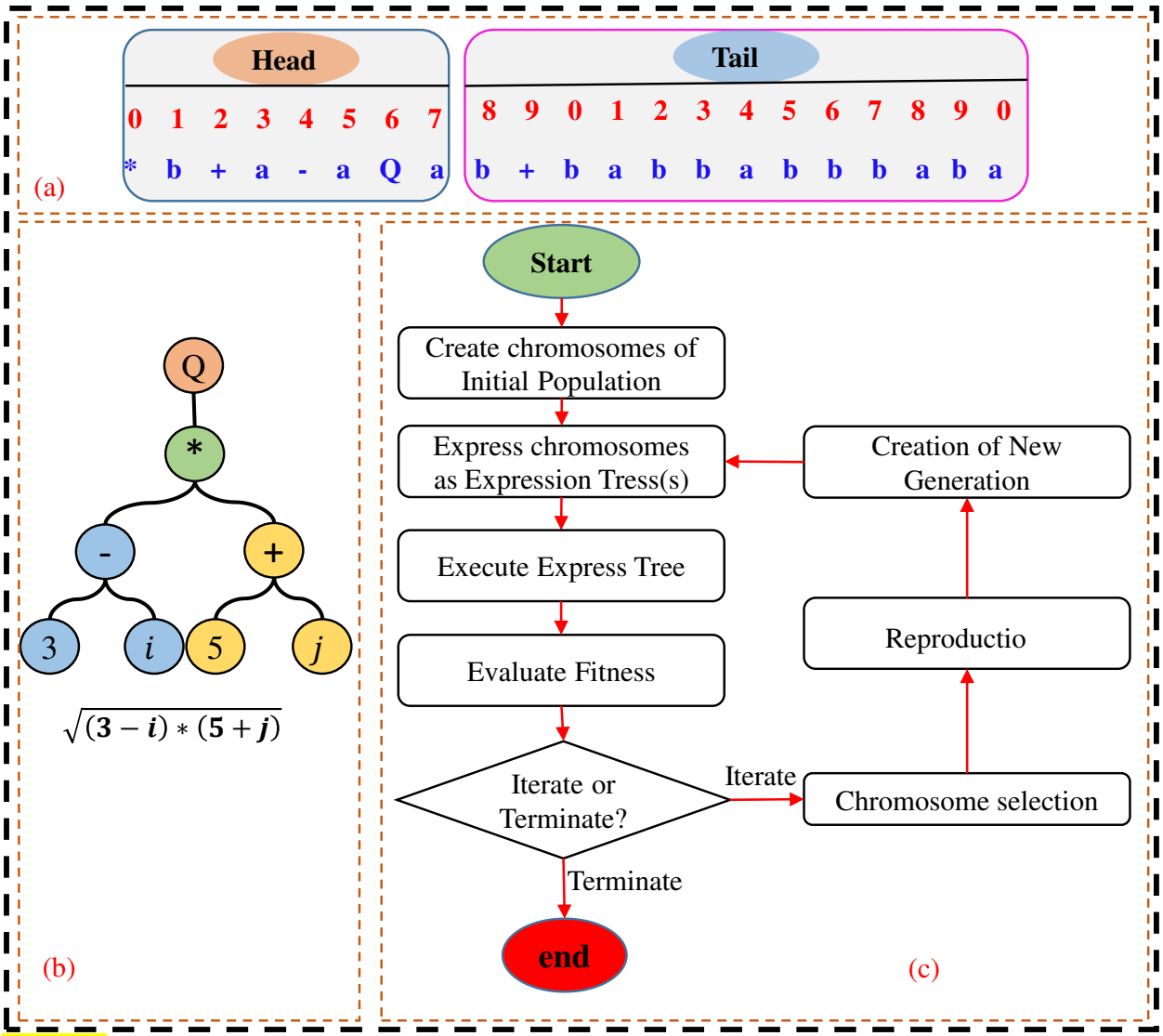

Figure 6. Schematic structure for GEP algorithm: (a) typical structure of a chromosome in GEP; (b) GEP model representing expression tree; (c) Basic working steps for the GEP model.

3. Performance measures

The accuracy of the developed models was measured using three statistical indicators, namely coefficient of determination (R^2), root mean square error (RMSE), and mean absolute error (MAE). These indices were selected due to their diverse functions in measuring the accuracy, reliability, and precision of models. They enable a more objective assessment of the model's performance in carrying out its designated tasks. RMSE represents the variation between the predicted and the measured values. RMSE is a common indicator employed in regression analysis to assess the accuracy of predictions in machine learning, and other applications. On the other hand, MAE measures the average size of estimating mistakes. The MAE indicates the average absolute difference between the predicted and true values of a sample. Typically, smaller values of RMSE and MAE indicate better performance and high accuracy. R^2 value indicates the degree to which a regression model's independent variables explain the dependent variable's output. R^2 plays a crucial role in assessing the goodness-of-fit of a regression model and comparing different ML models. A higher R^2 indicates a stronger degree of correlation between the model and the observed data, with a value close to 1 indicating better performance and higher accuracy. Equations used to calculate the value of these indices are listed in following equations:

$$RMSE = \sqrt{\frac{1}{n}\sum_{i=1}^{n} (y_i - \hat{y}_i)^2} \quad (2)$$

$$MAE = \frac{1}{n}\sum_{i=1}^{n} |y_i - \hat{y}_i| \quad (3)$$

$$R^2 = 1 - \frac{\sum_{i=1}^{n} (\hat{y}_i - y_i)^2}{\sum_{i=1}^{n} (\bar{y}_i - y_i)^2} \quad (4)$$

where n represent the total amount of data samples; $\hat{y}_i$is the predicted value of the ith sample; and y_i is the actual value of the ith sample.

4. Result and discussion

4.1. Experimental Results

This section presents the effects of each factor on interface bonding fatigue indices, quantified by interface shear stiffness (ISS) and interface fatigue life (IFL).

4.1.1. Effect of normal stress

To illustrate the influence of normal stress on interlayer fatigue properties, ISS and IFL were analyzed under a range of controlled testing conditions. Specifically, the experiments were conducted under distinct temperatures (15°C, 25°C, 35°C, and 45°C) to represent a wide range of thermal environments. Alongside, a constant shear stress of 196 Kpa and a fixed loading frequency of 10 Hz were maintained. Six different levels of normal stress were applied to comprehensively assess its impact. Figures 7 (a and b) display the results, effectively highlighting the correlation between varying levels of normal stress and their respective effects on ISS and IFL.

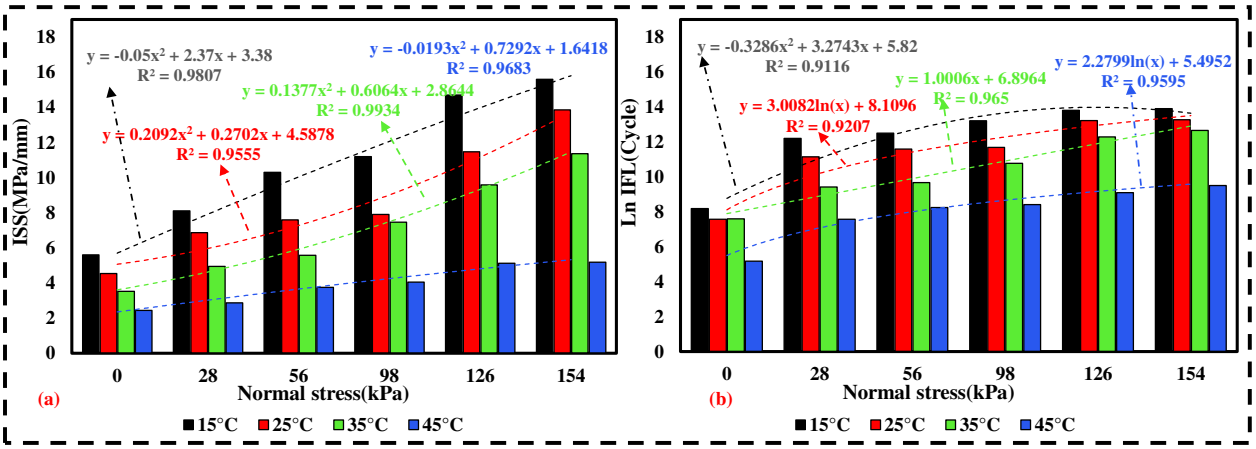

Figure 7. Effect of normal stress on: (a) ISS asphalt pavement; (b) IFL asphalt pavement.

The figure clearly demonstrates substantial increases in both ISS and IFL with increasing normal stress at all temperatures tested. Specifically, Figure 7(a) shows that increasing the normal stress from 0 to 154 kPa resulted in notable ISS increases of 178.5%, 204.9%, 222.3%, and 112.6% at 15°C, 25°C, 35°C, and 45°C, respectively. Similarly, Figure 7(b) shows that increasing the normal stress from 0 to 154 kPa led to substantial IFL increases of 69.9%, 75.1%, 66.8%, and 84.1% at the same temperatures. However, it is observed that at elevated temperatures, the

impact of increasing normal stress beyond 56 kPa becomes minimal on both shear stiffness and fatigue life. This phenomenon could be attributed to the fact that at higher temperatures, an increase in normal pressure may enhance friction between asphalt layers, thus improving fatigue life up to a certain point, beyond which further increases in normal stress do not significantly affect ISS and IFL.

To conclude, the application of normal stress, simulating tire contact pressure on the road surface, has a significant effect on interface shear stiffness and fatigue life. Neglecting this factor would underestimate the interlayer fatigue behavior between adjacent asphalt layers.

4.1.2. Effect of shear stress

To investigate the effect of shear stress on the interlayer fatigue performance in terms of ISS and IFL, various temperatures (15, 25, 35, and 45 °C), a constant normal stress of 126 kPa, and a consistent loading frequency of 10 Hz across six shear stress levels were examined, as displayed in Figure 8 (a and b).

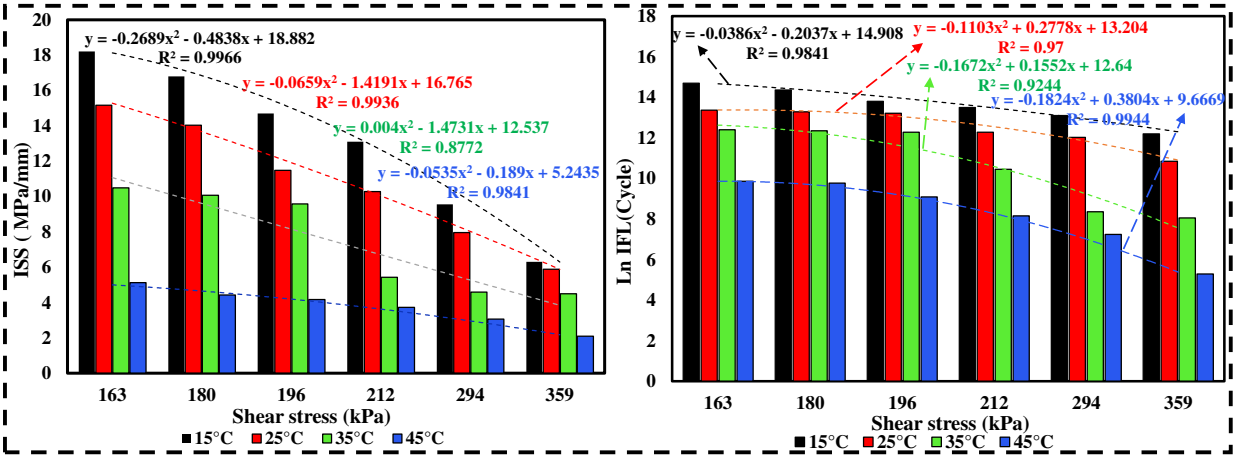

Figure 8. Effect of shear stress on: (a) ISS asphalt pavement; (b) IFL asphalt pavement.

Figure 8(a) reveals that increased shear stress leads to reduced shear stiffness. Notably, when shear stress rose from 163 kPa to 359 kPa, ISS values decreased by 65.4%, 61.2%, 57.2%, and

399 59.1% at temperatures of 15°C, 25°C, 35°C, and 45°C, respectively. It is clear that the difference
400 in shear stiffness at different temperatures is more pronounced at lower shear stress levels than at
401 higher stresses. This is likely due to decreased friction at the interface, leading to less resistance
402 to shear movement at lower temperatures as shear stress rises, resulting in a significant decline in
403 shear stiffness. Similarly, Figure 8(b) demonstrates that greater shear stress reduces the
404 interface's fatigue life at all temperatures. This means that as shear stress increases from 163 kPa
405 to 359 kPa, the fatigue life decreases by 17.0%, 18.9%, 35.1%, and 46.4% at temperatures of
406 15°C, 25°C, 35°C, and 45°C, respectively. The test results show that the estimated fatigue and
407 the relationship characterizing interface fatigue behavior at each temperature are well-represented
408 by a linear regression (quadratic form) with high R^2 values. As anticipated, higher shear stress
409 correlates with poorer fatigue performance at the interface for each temperature. Notably, the
410 decline in fatigue life due to shear stress at a higher temperature (45 °C) is more significant than
411 at lower temperatures.

412 *4.1.3. Effect of loading frequency*

413 The study also examined the impact of loading frequency on interlayer fatigue behavior. Various
414 temperatures (15, 25, 35, and 45 °C), a constant normal stress of 126 kPa, and a fixed shear stress
415 of 196 kPa were evaluated across five different loading frequency levels to assess their influence
416 on ISS and IFL, as depicted in Figures 9(a and b). Figure 9 (a) clearly demonstrates that an
417 increase in loading frequency results in a rise in ISS at all temperatures. This means, when the
418 loading frequency increased from 1 Hz to 10 Hz, ISS increased by 100.6%, 94.8%, 124.1%, and
419 83.1% for temperatures of 15°C, 25°C, 35°C, and 45°C, respectively. Notably, at high
420 temperature (45 °C), the variation in stiffness with frequency up to a loading frequency of 10 Hz

is not considerable, while at lower to normal temperatures (15–35 °C), one can observe a significant change in shear stiffness.

Figure 9 (b) illustrates a trending increase in fatigue life (IFL) with loading frequency. Specifically, the improvement in fatigue life from a loading frequency of 1 to 10 Hz accounts to an increase of 18.4%, 25.0%, 56.8%, and 58.3% for the respected temperatures of 15°C, 25°C, 35°C, and 45 °C. This enhanced fatigue resistance likely stems from asphalt's viscoelastic properties. At higher frequencies, the asphalt has less time to deform during each loading cycle, causing it to stiffen and become more elastic.

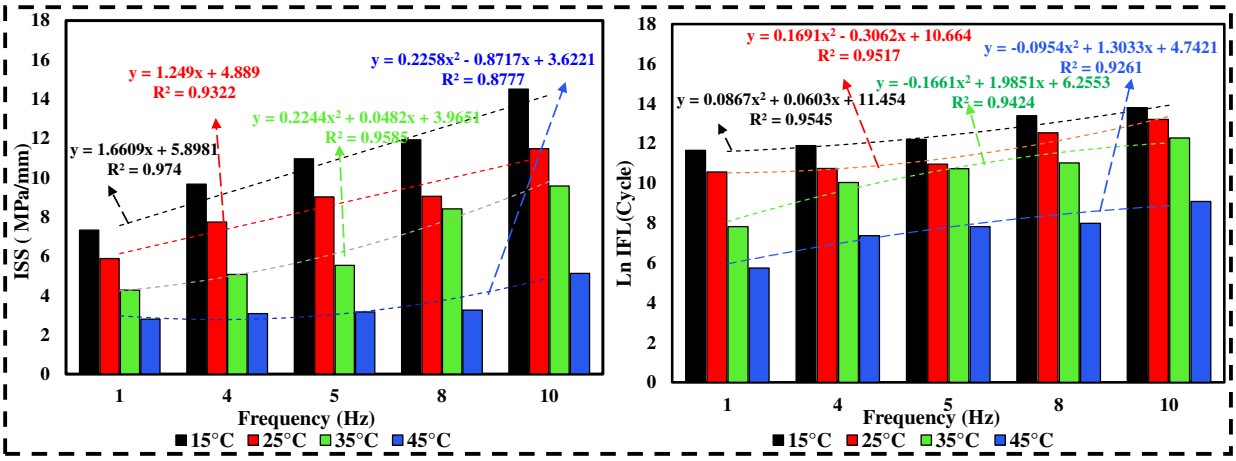

Figure 9. Effect of loading frequency on: (a) ISS asphalt pavement; (b) IFL asphalt pavement.

4.1.4. Effect of temperature

To study the effect of temperature on the interlayer fatigue properties, interface fatigue tests were conducted under given range of temperatures, a constant normal stress of 56 kPa, a constant shear stress of 196 kPa, and a fixed loading frequency of 10 Hz. Figure 10 presents the analysis results of temperature impacts on the ISS and the IFL. It is evident that temperature changes affect the ISS and IFL of asphalt pavement significantly. As the temperature increases from -10 to 45 °C, Figure demonstrates an 81.3% decline in ISS. Similarly, changing the test temperature from 0 to 45°C led to a 59.3% reduction in IFL. This phenomenon can be attributed to the viscoelastic nature of the interlayer bonding, where tack coat

material exhibits high sensitivity to temperature. As the temperature increases, asphalt binder softens continuously, leading to a gradual reduction to interface fatigue properties.

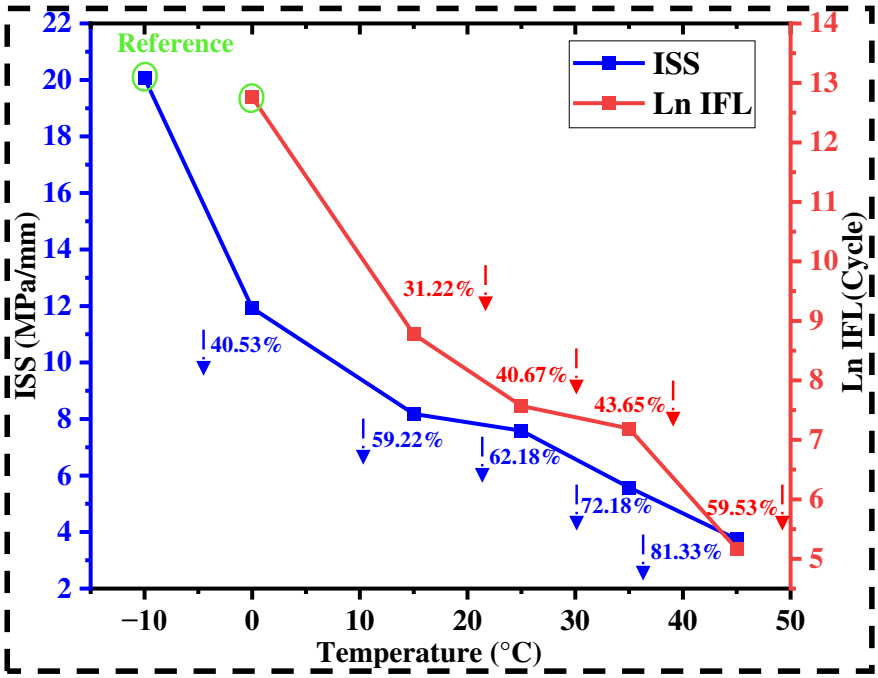

Figure 10. Effect of temperature on ISS and IFL of asphalt pavement.

4.2. Data Preparation

Following laboratory experiments, obtained data were analyzed and prepared for developing ML prediction models. Table 5 provides a summary of the descriptive statistical analysis results, presenting the statistical characteristics of the main parameters considered in this study. The models were developed using a total of 84 dataset, randomly divided into training dataset and testing dataset. The training dataset, comprising 70% of the total data, was utilized to construct the models while the remaining 30% was designated as the testing dataset, employed explicitly to assess and validate the model's capacity for generalization. To mitigate the impact of varying eigenvalue dimensions across samples on the models' predictive efficiency and accuracy, all input data underwent normalization before model training. This process utilized the min-max normalization method, as outlined by Tenpe and Patel (2020), ensuring uniformity across the dataset and enhancing the reliability of our predictions.

Table 5. Descriptive statistical analysis

Variable	N	Unit	Description	Mean	Standard deviation
T	84	°C	Temperature	27.74	13.72
N	84	kPa	Normal stress	95.56	46.75
F	84	Hz	Frequency	8.262	3.117
SF	84	kPa	Shear stress	243.0	76.30

4.3. Result of ANN application

Using MATLAB 2019b, the appropriate feed-forward ANN models were built and trained to predict the ISS and IFL of asphalt pavement. Many networks are trained with different settings of hidden layers, hidden nodes, epochs, and types of activation functions to reach the optimal configurations with the highest accuracy. Table 6 summarizes the best hyperparameters used for the modeling of ANNs. Furthermore, Figure 11 shows the architecture of the proposed ANN models for both the ISS and IFL. This figure presents the optimized ANN model, achieved through an iterative process of trial and error, involving adjustments to the number of hidden neurons, layer activation functions, and bias connections to ensure optimal performance. The optimal architecture of the ANNs, which yielded the most accurate predictions, incorporated a single hidden layer with 7 neurons for ISS and 10 neurons for IFL. The highest performance was achieved using the Levenberg-Marquardt training algorithm, after 20 epochs for ISS and 13 epochs for IFL, respectively. Additionally, the networks utilized the hyperbolic tangent sigmoid (TANSIG) as the activation function in the hidden layer and the linear (purelin) function in the output layer, effectively enhancing the model's predictive capabilities.

Table 6. The best ANN-model hyper-parameters

ANN parameters	Type / Best value	
	ISS	IFL
Neural network model used	Feed forward	Feed forward
Number of hidden layers	1	1
Number of neurons of each hidden layer	7	10
Network	4-7-1	4-10-1

Learning algorithm	The Levenberg-Marquardt backpropagation	The Levenberg-Marquardt backpropagation
Activation function for hidden layer	TANSIG	TANSIG
Activation function for output layer	PURELIN	PURELIN
Data division	Random basis	Random basis
Data division and number (training–testing)	70%-30% (59-25)	70%-30% (59-25)
Applied epochs	20	13
Learning rate	0.001	0.001

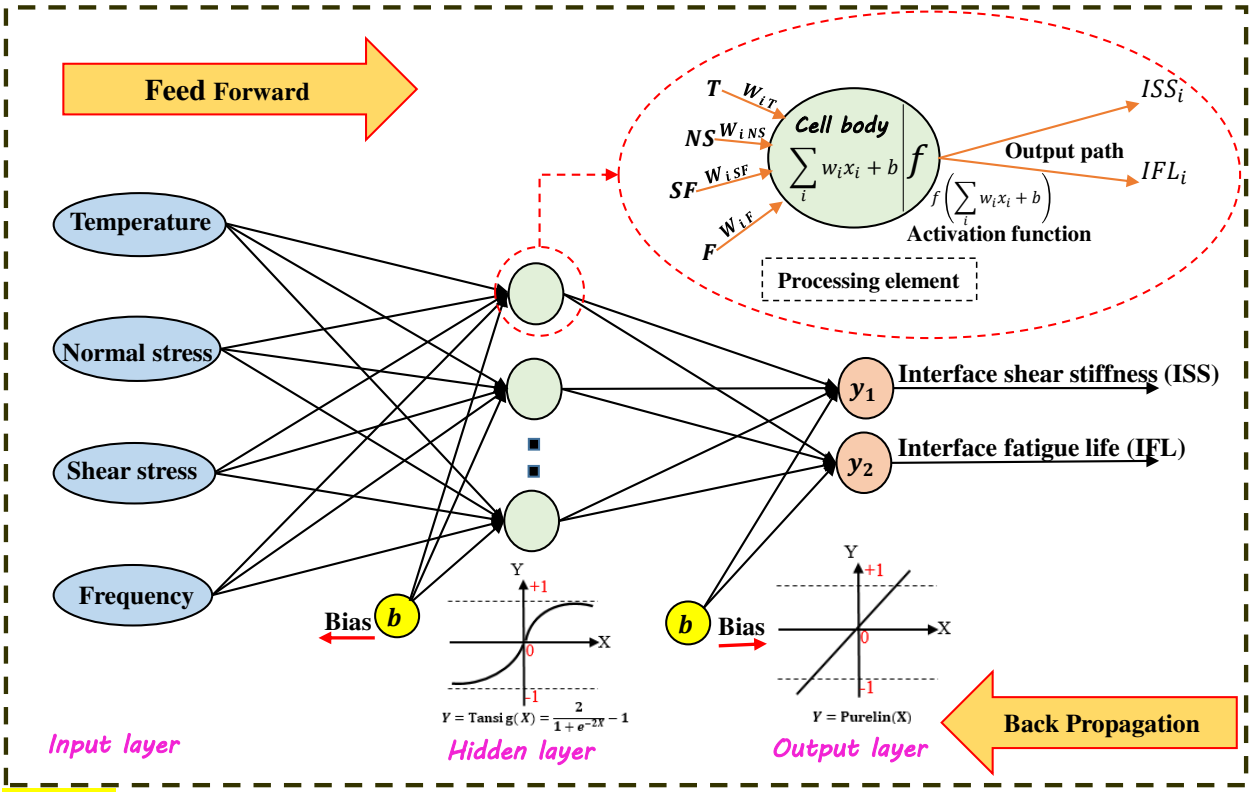

Figure 11. ANN architecture of the predicted models for the ISS and IFL of asphalt pavement.

The ANN regression plots comparing experimental and predicted values for ISS of pavement during both training and testing phases are shown in Figure 12 (a and b). The overall R^2 values, exceeding 0.97 (0.980 for training and 0.972 for testing), underscore the proposed ANN model's exceptional predictive accuracy. Figures 12 (c and d) visually represent the proposed ANN model's performance and error margin by comparing predictions against experimental results. These findings underscore the model's remarkable consistency with true values, highlighting its well-calibrated nature and robust generalization capabilities.

Such attributes signify the model's adeptness at handling new and unseen data effectively. Moreover, RMSE and MAE metrics were recorded at 0.8264 and 0.6363 for the training set, and 1.0607 and 0.8167 for the testing set, respectively, indicating minimal discrepancy between the predicted and observed values.

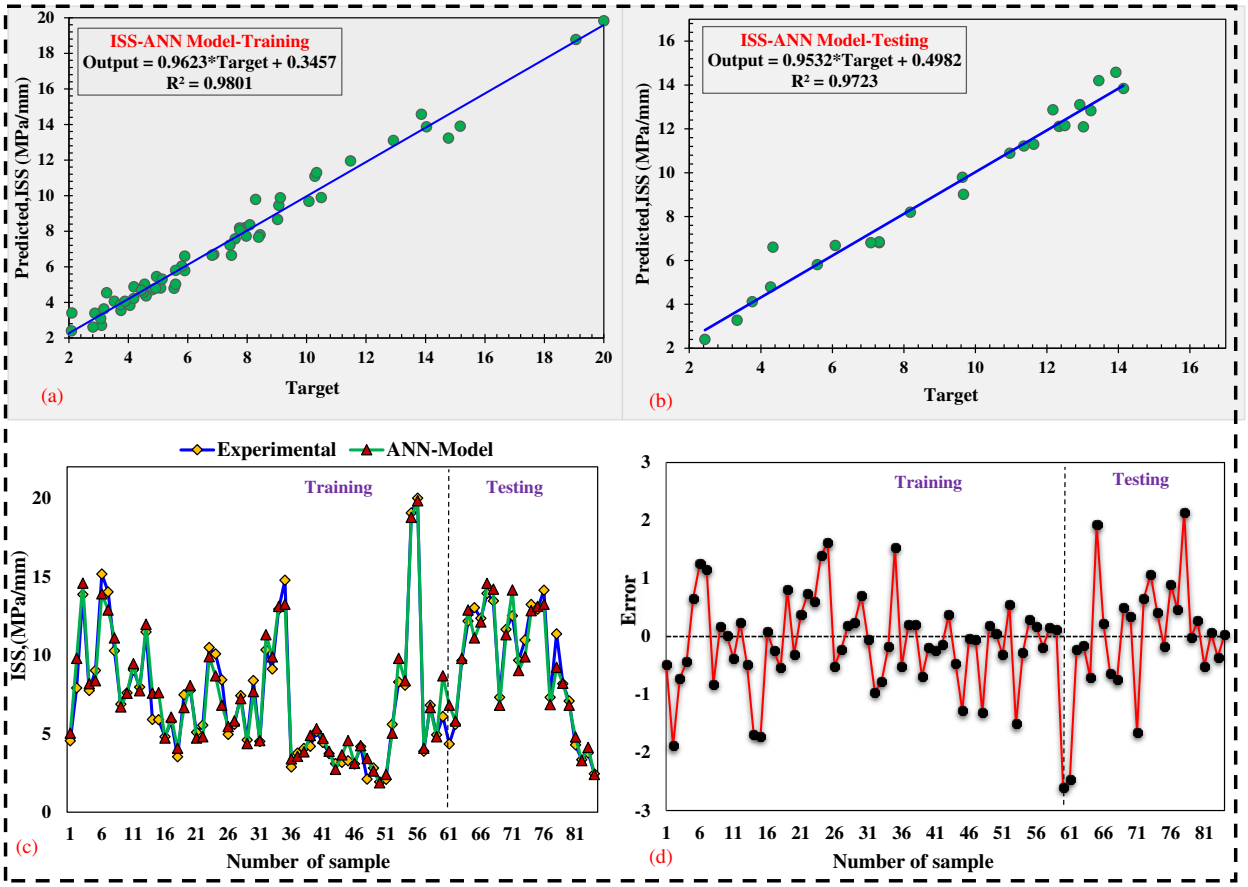

Figure 12. The proposed ANN model for ISS: (a) regression plot for training; (b) regression plot for testing; (c) performance of the model; (d) error range.

Similarly, the relationships between actual and predicted IFL values by the ANN approach are shown in Figure 13 (a and b) during both the training and testing phases. It can be noted that R^2 values in training and testing sets are 0.972 and 0.943, respectively. These results indicate that the developed ANN model for IFL can explain more than 94% of the measured data and can be used effectively to predict the IFL of asphalt pavement accurately. Figure 13 (c and d) graphically illustrate the performance and error range of the developed ANN model for IFL by comparing predictions with experimental results. As can be seen,

the developed ANN prediction model for the IFL is very consistent with the actual values, denoting that the developed ANN model for IFL has been well-trained and can be generalized well. In other words, the model has the potential to perform effectively on new and unseen data. Moreover, the RMSE and MAE values were computed to be 0.4987 and 0.3839 for the training dataset, and 0.7555 and 0.5817 for the testing dataset, respectively. These values indicate a relatively minor discrepancy between the predicted and measured values.

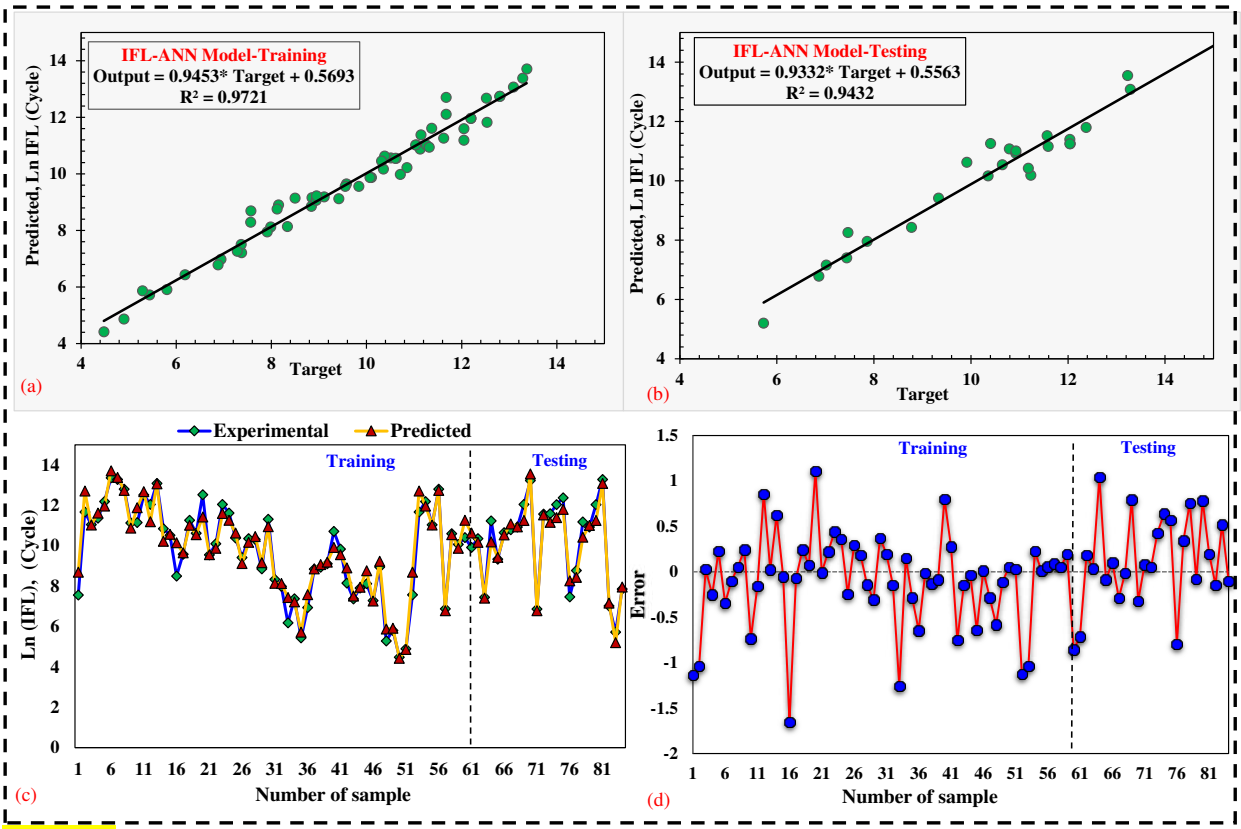

Figure 13. The proposed ANN model for IFL: (a) regression plot for training; (b) regression plot for testing; (c) performance of the model; (d) error range

4.4. Result of GEP application

The GEP model, aimed at predicting the ISS and IFL, utilized the identical dataset as that for the ANN model training. Developed with GeneXproTools version 5.0 (Ferreira 2001, 2006), the GEP model underwent multiple iterations to identify the most effective parameter configuration. Parameters such as the number of chromosomes, genes, head size, mutation rate, and linking functions were thoroughly

adjusted to refine the model's performance. The selection of the optimal GEP model was guided by a multi-objective strategy that balanced model simplicity against the precision of its predictions, both during training and validation stages. This method was in harmony with the empirical findings of this research, ensuring the GEP model's parameters were fine-tuned for accuracy. Details of the optimized GEP model parameters are presented in Table 7, showcasing the rigorous process behind its development.

Table 7. The optimal GEP-model hyper-parameters

GEP parameters	Type / Settings	
	ISS	IFL
Chromosome's number	30	30
Gene's number	3	3
Head's size	8	8
Linking functions	Addition	Addition
Used function set	+, - , * , /, Exp, Ln	+, - , * , /, X^2
Fitness	1000	1000
Inversion rate	0.00546	0.00546
Mutation rate	0.00138	0.00138
Gene recombination and transposition rate	0.00277	0.00277
One-point and two-point recombination rate	0.00277	0.00277
Data division and number (training–testing)	70%-30% (59-25)	70%-30% (59-25)

The output of the GEP model to predict the ISS of asphalt pavement is demonstrated as an expression tree (ET) in Figure 13. The best performing GEP model for the ISS prediction is shown as the mathematical expression of Y1+Y2+Y3:

$$Y1 = \left[\left(\frac{N}{SF} - (-3.2068 - N)\right) - N\right] + \left(\frac{F}{6.9015}\right)^{e} \quad (5)$$

$$Y2 = \frac{T}{-2.6441 + \left(\frac{-89.4741)}{N - SF}\right)} \quad (6)$$

$$\mathrm{Y3} = \ln\left(SF - \left(303.076 - (T^2 + N^2)\right)\right) \quad (7)$$

Figures 14 (a and b) present the GEP regression plots, showcasing the correlation between experimental and predicted values for the ISS of asphalt pavement across both training and testing datasets. A notable R^2 value of 0.921 for the training dataset reflects the GEP model's predictive accuracy for ISS, mirroring the experimental data closely. Similarly, for the testing dataset, an R^2 value of 0.913 demonstrates a strong correlation between the predicted ISS values and the actual observations. Figures 14 (c and d) further illustrate the efficacy of the GEP model in predicting ISS, comparing its predictions with the empirical results and highlighting the error range. The alignment between the GEP model's predictions and real-world data is evident, showcasing the model's effective training and generalization prowess. Furthermore, RMSE and MAE were calculated, yielding 1.4020 and 1.0795 for the training set, and 1.4911 and 1.1481 for the testing set, respectively. These metrics indicate a relatively small discrepancy between the predicted and actual values, affirming the GEP model's capability to accurately predict ISS behavior with commendable precision.

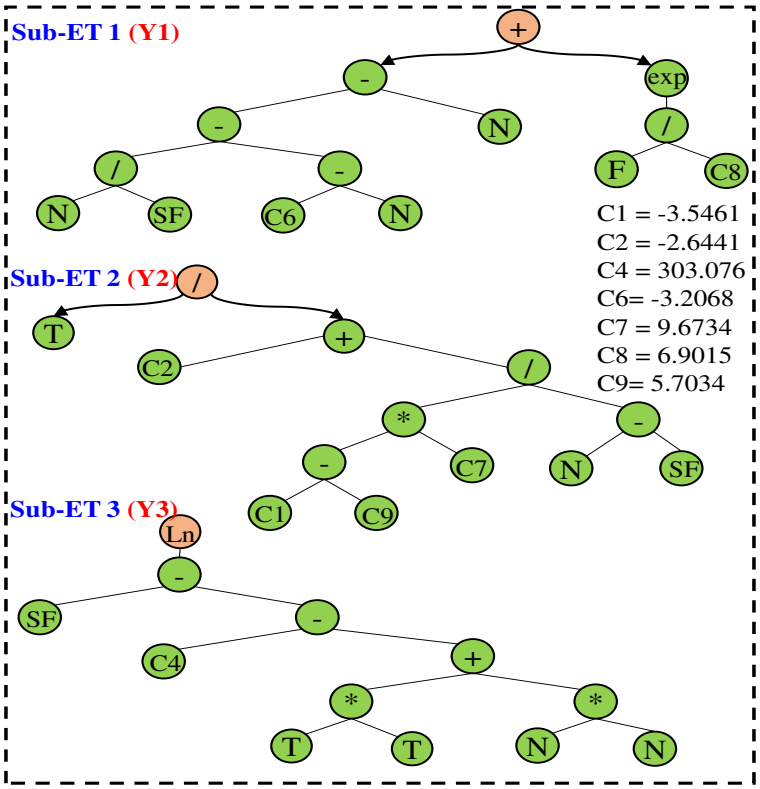

Figure 13. The output of GEP model as Expression tree for the ISS.

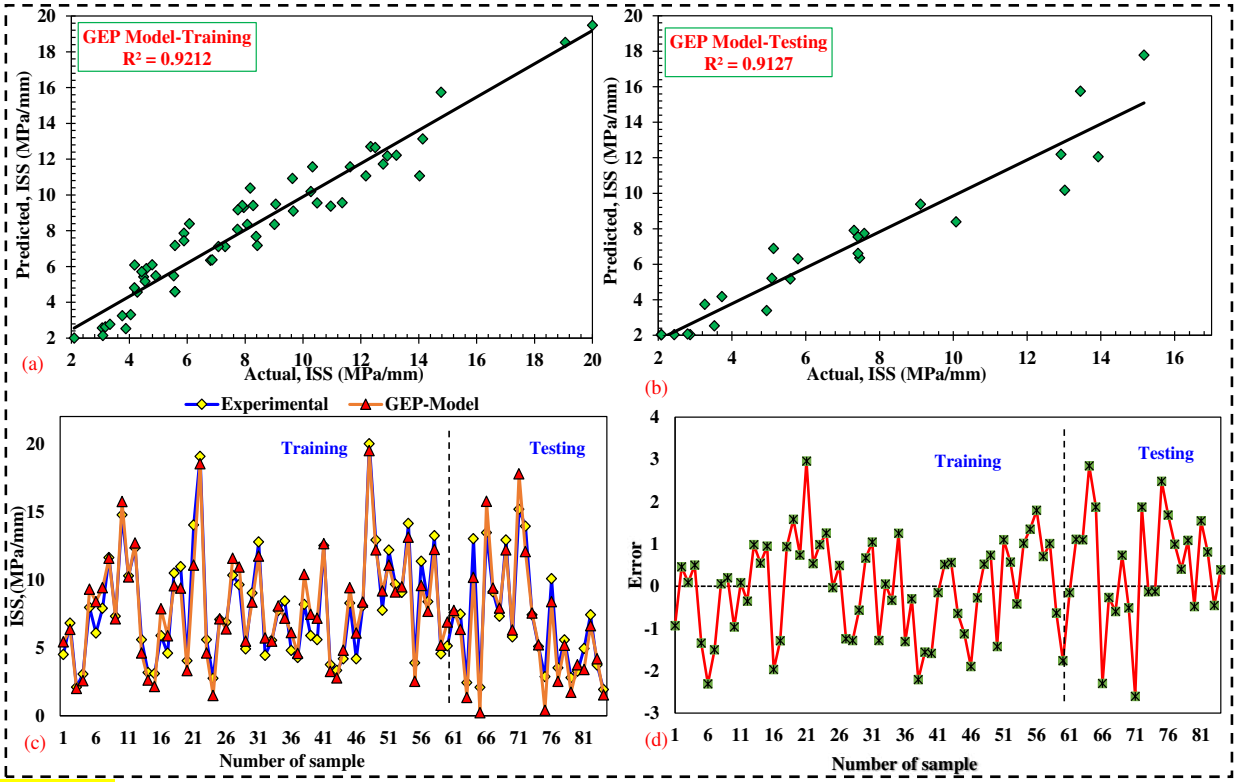

Figure 14. The proposed GEP model for ISS: (a) regression plot for training; (b) regression plot for testing; (c) performance of the model; (d) error range.

In a similar way, the output of the GEP model for predicting the IFL of asphalt pavement is shown in the form of an ET, as depicted in Figure 15. The figure illustrates that the most effective GEP model in predicting IFL can be represented as the mathematical expression of Y1+Y2+Y3:

$$Y1 = \left(\frac{T+N}{SF} \times (-5.6752)\right) - (7.8764 + T) \quad (8)$$

$$Y2 = T - \left(\frac{T^2}{370.4507} - 4.7017\right) \quad (9)$$

$$Y3 = 5.7034 - \frac{T}{\frac{F^2}{1.9592} + (F + 8.3517)} \quad (10)$$

Figure 16 (a and b) display the relationships between the actual and predicted IFL values generated using the GEP technique during both the training and testing stages, respectively. It can be seen that the R^2 values for training and testing datasets are 0.913 and 0.90, respectively. These outcomes signify that the

developed GEP model for IFL can account for over 90% of the observed data, demonstrating its efficacy in providing accurate predictions for the IFL. Figure 16 (c and d) further exhibits the performance of this GEP model, comparing its predictions with experimental results and the associated error range. Clearly, the GEP model's predictions for IFL closely align with the actual values, demonstrating a well-trained model with robust generalization capabilities. In addition, the RMSE and MAE values have been computed, resulting in 0.6231 and 0.4797 for the training dataset, and 0.6492 and 0.5107 for the testing dataset, respectively. These figures highlight a relatively minimal disparity between the model's predictions and the actual results, signifying the model's high level of accuracy.

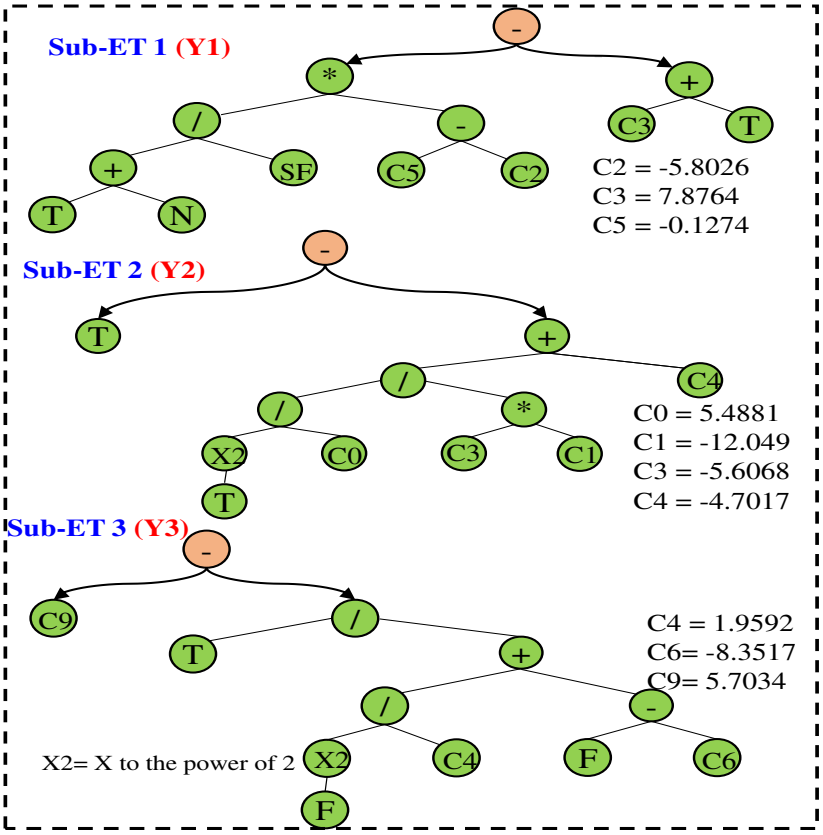

Figure 15. The output of GEP model as Expression tree for the IFL.

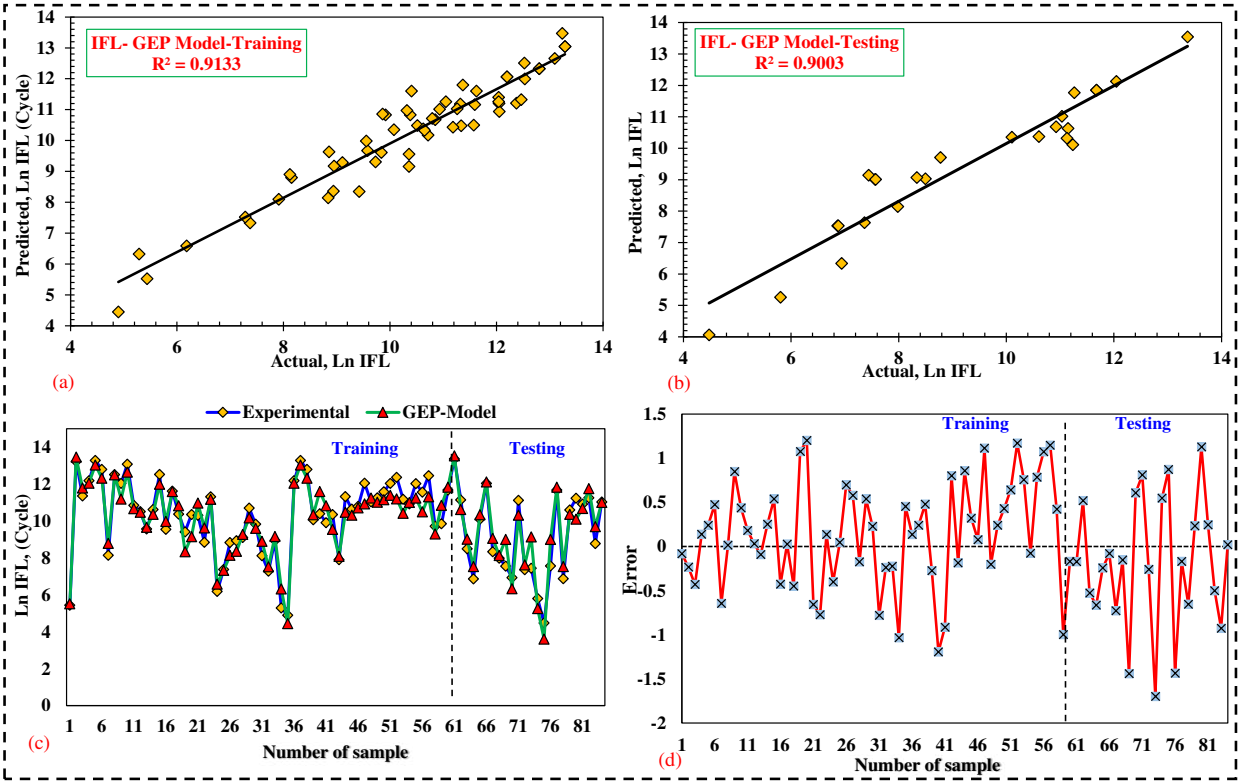

Figure 16. The proposed GEP model for IFL: (a) regression plot for training; (b) regression plot for testing; (c) performance of the model; (d) error range

To conclude, statistical performance indices for all proposed models are summarized in Table 8. These results clearly demonstrate the effective training of the models and the presence of a strong correlation between the predicted and experimental output, coupled with low error values. In other words, no overfitting is apparent for all proposed models, indicating a higher generalization capacity and ability to predict reliable results for unseen data.

Table 8. Comparative analysis for performance indices of the proposed models.

ANN model	Training			Testing		
	RMSE	MAE	R^2	RMSE	MAE	R^2
Interface Shear Stiffness (ISS)	0.8264	0.6363	0.9801	1.0607	0.8167	0.9723
Interface Fatigue Life (IFL)	0.4987	0.3839	0.9721	0.7555	0.5817	0.9432
GEP model						
Interface Shear Stiffness (ISS)	1.4020	1.0795	0.9212	1.4911	1.1481	0.9127

Interface Fatigue Life (IFL)	0.6231	0.4797	0.9133	0.6492	0.5107	0.9003

4.5. Sensitivity analysis

To validate the comprehensiveness of the proposed prediction models, a sensitivity analysis was performed. This analysis assessed the impact of varying independent variables on the predicted interlayer bonding fatigue indices, within a defined framework of assumptions. Through this process, the significance and effect of each input parameter on the model outcomes were thoroughly evaluated, providing insights into their relative importance and contribution to the predictive accuracy of the models.

4.5.1. Input parameter analysis based on proposed model

Figure 17 (a, b, and c) presents the variation of ISS varies under diverse testing scenarios. Figure 17 (a) depicts the ISS changes across three temperature conditions (25, 35, and 45 °C) with a set shear stress of 196 kPa and a loading frequency of 10 Hz, as normal stress levels are adjusted. The results clearly demonstrate a marked increase in ISS across all temperature ranges when normal stress rises from zero to higher levels. Furthermore, Figure 17 (b) exhibits ISS changing trend at varying shear stress levels while holding three temperature scenarios (25, 35, and 45 °C), a consistent normal stress of 126 kPa, and a fixed loading frequency of 10 Hz. The data presented clearly indicate that an increase in shear stress corresponds to a decline in shear stiffness across all temperature settings. Lastly, Figure 17 (c) examines the impact of altering loading frequency levels on ISS, under the same three temperatures (25, 35, and 45 °C), maintaining a normal stress of 126 kPa and a constant shear stress of 196 kPa. The illustration distinctly shows that an increase in loading frequency results in a rise in ISS , applicable to all temperature conditions.

A noteworthy finding from Figure 17 (a, b, and c) is the notable consistency observed between the predicted values produced by the proposed prediction models (ANN and GEP) for ISS and the corresponding experimental data. This harmonious alignment in ISS predictions, achieved through both

ANN and GEP models, highlights the models' precision and dependability in reflecting real-world scenarios within the specified range.

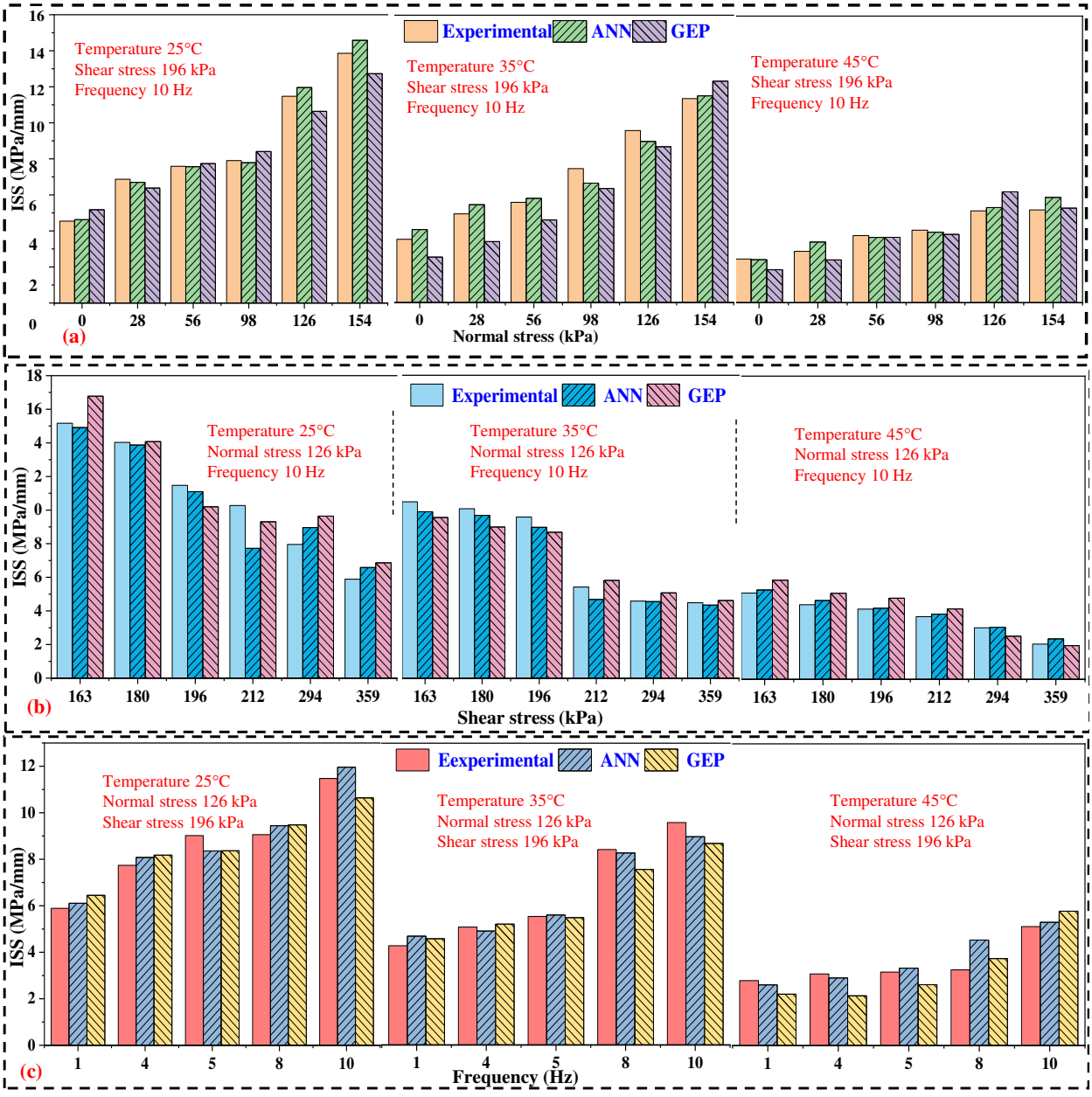

Figure 17. Analysis result of inputs parameter on the ISS under different condition based on the proposed ANN and GEP models: (a) normal stress; (b) shear stress; (c) loading frequency.

Similarly, Figure 18 (a, b, and c) illustrates the variation in IFL under different test conditions. Figure 18 (a) shows the IFL changes with different normal stress levels under three temperature environments (25, 35, and 45 °C), paired with a shear stress of 196 kPa and a loading frequency of 10 Hz. It is clearly

observed that IFL increases under all temperature settings when normal stress levels are elevated. In Figure 18 (b), the impact of varying shear stress levels on IFL is presented, while temperatures remain stable (25, 35, and 45 °C), alongside a fixed normal stress of 126 kPa and a constant loading frequency of 10 Hz. This segment of the figure demonstrates that an increase in shear stress is associated with a decline in IFL under all temperatures. Lastly, Figure 18 (c) explores the IFL response to different loading frequencies, set against the backdrop of the same temperature conditions (25, 35, and 45 °C), with a constant normal stress of 126 kPa and a fixed shear stress of 196 kPa. This illustration clearly shows that increasing the loading frequency results in an increase in IFL in all temperature scenarios. Moreover, it is evident that the predicted values for the IFL generated by the ANN and GEP models closely match the experimental data. This alignment in predictions underscores the accuracy and dependability of both models in mirroring real-world conditions within their defined parameters.

In summary, the remarkable consistency between the model predictions and experimental data across diverse conditions, as demonstrated in Figures 17 and 18, affirms the effectiveness of the ANN and GEP models. Furthermore, these results offer crucial insights into the interface fatigue behavior under service loads. Through a detailed analysis, the models and experiments contribute significantly to comprehension of the impact of temperature and loading conditions on interlayer fatigue behavior, enhancing the ability to predict and mitigate potential pavement failures.

This understanding is pivotal for creating durable pavement designs and implementing maintenance strategies that promote the durability and sustainability of road infrastructure. Quantifying the effects of environmental factors and loading conditions on interface bonding will pave the way for enhancing fatigue resistance through structural improvements, informed materials selection, and targeted interface modifications. Collectively, the comprehensive integration of modeling and experimental approaches drives the capability to precisely predict interface fatigue performance, thereby optimizing asphalt pavement constructions for prolonged service life and efficiency.

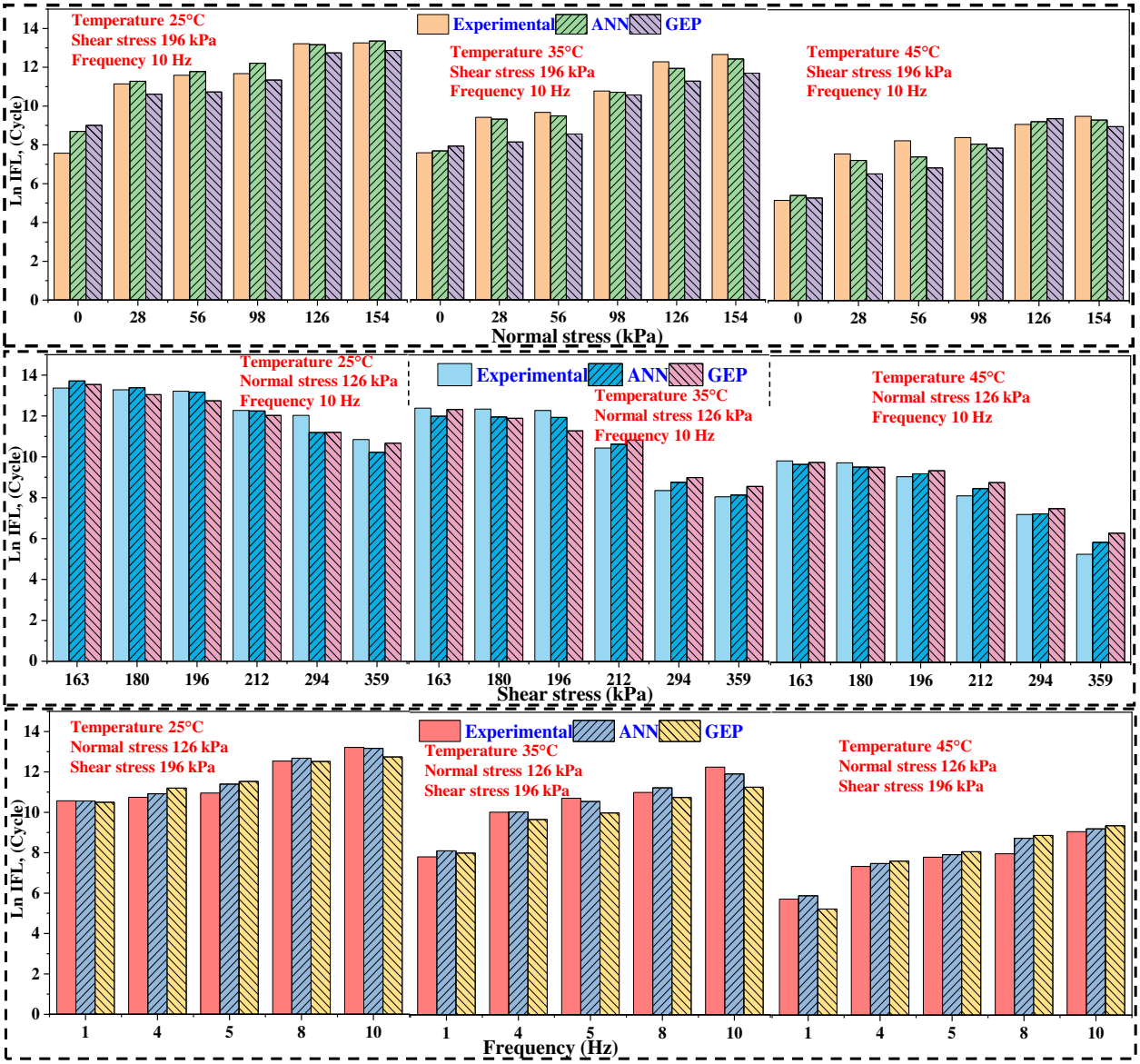

Figure 18. Analysis result of inputs parameter on the IFL under different condition based on the proposed ANN and GEP models: (a) normal stress; (b) shear stress; (c) loading frequency

4.5.2. Significance of variables

The superior performance of the proposed ANN models for interface fatigue indices has led to their use in assessing the significance of input variables. These variables were examined based on their influence on the output variables (ISS and IFL), with the impact of each variable clearly determined. To quantify the importance of these input variables, the Error Method has been applied. This approach calculates the ratio

of the model's error with the exclusion of a specific (i-th) variable to the error recorded when all input variables are present. This ratio effectively highlights the importance of the i-th variable in the model's predictive accuracy, as outlined by Ehsani et al. 2023 and Mrzygłód et al. 2020. The following is the corresponding formula:

$$W_i = \frac{MSE_i}{MSE} \quad (11)$$

where W_i is the variable importance measure of the ith variable; MSE is the error produced from the model when all variables are included; and MSE_i is the error produced from the model when the i-th variable is excluded from the model.

Figure 19 illustrates the variable importance as determined by the proposed ANN models, showcasing that temperature (T) significantly impacts both ISS and IFL. In the context of ISS, shear stress (SF) and normal stress (N) are identified as the second and third most influential factors, respectively. In contrast, for IFL, N and SF stand out as the second and third most crucial variables. Frequency (F) is highlighted as the least influential variable affecting both ISS and IFL. According to Mrzygłód et al. (2020), a variable is considered non-essential if its importance weight (Wi) is below 1. In this analysis, however, all input parameters recorded Wi values above 1, underscoring that the variables were accurately identified and validated for their significance.

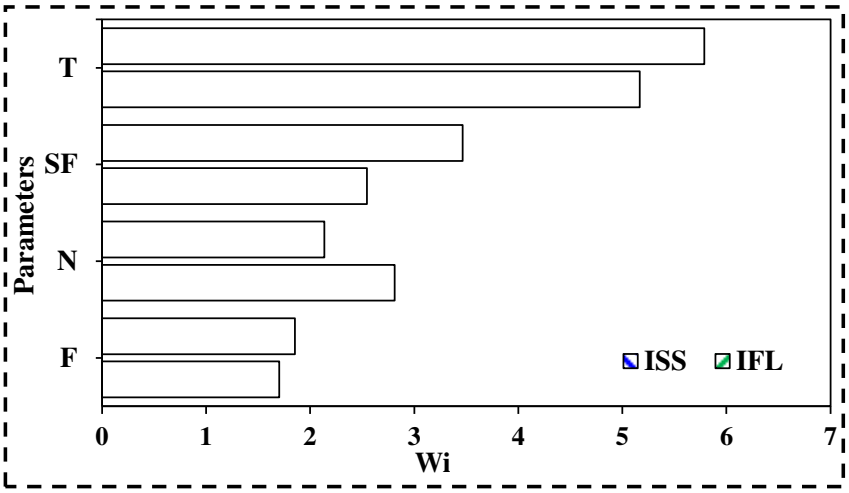

Figure 19. Variable importance for ISS and IFL.

5. Summary and conclusions

This study is a pioneering effort by introducing a novel integrated framework that combines two supervised ML techniques, namely artificial neural networks (ANNs) and gene expression programming (GEP) for the prediction and evaluation of interlayer fatigue properties in asphalt pavement. The assessment focused on two key indices, including interface shear stiffness (ISS) and interface fatigue life (IFL). 84 laboratory specimens were produced and tested using 4PST set-up under selected sets of testing conditions. R^2, RMSE, and MAE were utilized as statistical indices to evaluate the overall performance of the developed models. Additionally, the models were tested for universality to provide a theoretical basis for assessing the interlayer fatigue behavior of asphalt pavement, and sensitivity analysis confirmed their reliability. Based on the findings presented in this paper, the following conclusions can be drawn:

- The proposed ANN model achieved good results in predicting the ISS and IFL of asphalt pavement. It was found that the models developed using the ANN technique attained R^2 values of 98.0% and 97.2% for the training and testing datasets, respectively, for ISS. Moreover, for IFL of the pavement, the ANN-based models achieved R^2 values of 97.2 % and 94.3% in the respective training and testing sets. For the ISS-ANN model, the RMSE values were computed to be 0.8264 for the training set and 1.0607 for the testing set. The MAE values for the same model were 0.6363 for training set and 0.8167 for testing set. On the other hand, for the IFL-ANN model, the RMSE values were 0.4987 for training set and 0.7555 for testing set, while the MAE values were 0.3839 for training set and 0.5817 for testing set. Hence, the developed ANN model for both ISS and IFL has been well-trained and demonstrates strong generalization capabilities.
- The developed GEP model for ISS and IFL could explain more than 90% of the measured data. RMSE and MAE values were computed for the ISS-GEP model, resulting in 1.4020 for training and 1.4911 for testing for RMSE, and 1.0795 for training and 1.1481 for MAE. In the meantime, for the IFL-GEP model, the RMSE values were 0.6231 for training and 0.6492 for testing, and the MAE values were

685 0.4797 for training and 0.5107 for testing. These results suggest that the proposed GEP model can be
686 used effectively to predict ISS and IFL behavior with high accuracy.
687 • The results of testing the models for universality revealed that the predicted values of ISS and IFL
688 generated by both proposed prediction models demonstrated a comparable change trend and closely
689 align with the experimental data.
690 • With increasing normal stress from zero to higher values, a significant increase was observed in both
691 the ISS and IFL. Specifically, elevation of the normal stress from zero to 154 kPa resulted in ISS
692 increases of 178.5%, 204.9%, 222.3%, and 112.6% at respected temperatures of 15°C, 25°C, 35°C, and
693 45°C. Meanwhile, IFL exhibited increases of 69.9%, 75.1%, 66.8%, and 84.1% for the same
694 temperature levels when normal stress was increased in the specified range.
695 • Higher shear stress levels resulted in lower shear stiffness and fatigue life of the interface at all
696 temperatures. When the shear stress was increased from 163 kPa to 359 kPa, the ISS experienced
697 declines of65.4%, 61.2%, 57.2%, and 59.1% at temperatures of 15°C, 25°C, 35°C, and 45°C,
698 respectively. Moreover, the rate of IFL decreased by17.0% 18.9%, 35.1%, and 46.4% for the same
699 temperature levels when the shear stress was raised in the specified range.
700 • When loading frequency was elevated from 1 Hz to 10 Hz, the ISS raised by 100.6%, 94.8%, 124.1%,
701 and 83.1%, at temperatures of 15°C, 25°C, 35°C, and 45°C, respectively. Concurrently, the rate of
702 fatigue life (IFL) increased by 18.4%, 25.0%, 56.8%, and 58.3% for the same temperature levels when
703 the loading frequency increased in the specified range.
704 • Temperature changes had a substantial effect on both the ISS and IFL in asphalt pavement. Specifically,
705 as the temperature increased from -10 to 45 °C, the ISS declined by 81.3%. Similarly, changing the test
706 temperature from 0 to 45°C resulted in a reduction in IFL by 59.3%.
707 In summary, the findings of this research could make a pivotal contribution to interlayer bonding
708 designs in asphalt pavements. However, it is acknowledged that broadening the experimental dataset
709 will further refine the predictive accuracy of the models developed using hybrid machine learning

approaches. Furthermore, this study was limited to using a single tack coat type and application rate. Therefore, future research will aim to explore a more diverse range of tack coat types and application rates. This expansion will also include an examination of other critical factors such as aging and moisture effects, offering a deeper and more comprehensive understanding of interface fatigue behavior.

Data Availability Statement

The data supporting the models in this paper, as well as other findings of this study, are available from the corresponding author upon reasonable request.

Disclosure statement

The authors declare that there is no conflict of interest.

References

Alae, M., et al., 2020. Effects of layer interface conditions on top-down fatigue cracking of asphalt pavements. *International Journal of Pavement Engineering*, 21 (3), 280–288.

AL-Jarazi, R., et al., 2023. Development of prediction models for interlayer shear strength in asphalt pavement using machine learning and SHAP techniques. Road Materials and Pavement Design, 1-19

Al-Jarazi, R., et al., 2024. Interface Bonding Strength between Asphalt Pavement Layers under Mixed Shear-Tensile Mode: Laboratory Evaluation and Modeling Predictions. Journal of Materials in Civil Engineering, 36(2), 04023565.

Ashteyat, A., et al., 2020. Compressive strength prediction of lightweight short columns at elevated temperature using gene expression programing and artificial neural network. *Journal of Civil Engineering and Management*, 26 (2), 189–199.

Basheer, I. A., and Hajmeer, M., 2000. Artificial neural networks: Fundamentals, computing, design, and application. *Journal of Methods Microbiological Journal of Microbiological Methods*, 43(1), 3–31.

Code of China, 2004. Technical Specifications for the Construction of Highway Pavements. *Research Institute of Highway Ministry of Transport*. Beijing.

D'Andrea, A. and Tozzo, C., 2016. Interface stress state in the most common shear tests. *Construction and Building Materials*, 107, 341–355.

Dao, D. Van., et al., 2022. Prediction of interlayer shear strength of double-layer asphalt using novel hybrid artificial intelligence models of ANFIS and metaheuristic optimizations. *Construction and Building Materials*, 323, 126595.

De Bondt, A.H., 1999. Anti-reflective cracking design of (reinforced) asphaltic overlays. doctoral thesis. Delft University of Technology, Delft, South Holland, Netherlands.

741 Diakhaté, M., et al., 2011. Experimental investigation of tack coat fatigue performance: Towards an
742 improved lifetime assessment of pavement structure interfaces. *Construction and Building Materials*,
743 25 (2), 1123–1133.

744 Ehsani, M., et al., 2023. Optimized prediction models for faulting failure of Jointed Plain concrete
745 pavement using the metaheuristic optimization algorithms. *Construction and Building Materials*,
746 364: 129948.

747 Ferreira, Cândida., 2001. Gene Expression Programming: A New Adaptive Algorithm for Solving
748 Problems. Complex Systems, 13 (2), 87–129.

749 Ferreira, Cândida., 2006. *Gene Expression Programming Mathematical Modeling by an Artificial*
750 *Intelligence*. Springer.

751 Gandomi, A.H. and Roke, D.A., 2015. Assessment of artificial neural network and genetic programming
752 as predictive tools. *Advances in Engineering Software*, 88, 63–72.

753 Gao, W., 2018. A comprehensive review on identification of the geomaterial constitutive model using the
754 computational intelligence method. *Advanced Engineering Informatics*.

755 Guo, C., Wang, F., and Zhong, Y., 2016. Assessing pavement interfacial bonding condition. *Construction*
756 *and Building Materials*, 124, 85-94.

757 Hun, M., Chabot, A., and Hammoum, F., 2012. *A Four-Point Bending Test for the Bonding Evaluation of*
758 *Composite Pavement*.

759 Johnson, E.N., Melissa K. Cole, and John Pantelis, 2015. *Tack Coat Testing – Measuring Field Bond*
760 *Strength*.

761 Kara, I.F., 2013. Empirical modeling of shear strength of steel fiber reinforced concrete beams by gene
762 expression programming. *Neural Computing and Applications*, 23 (3–4), 823–834.

763 Kim, H., et al., 2011. Numerical and experimental analysis for the interlayer behavior of double-layered
764 asphalt pavement specimens. *Journal of Materials in Civil Engineering*, *23*(1), 12-20

765 Khweir, K., et al., 2003. Influence of layer bonding on the prediction of pavement life. *Proceedings of the*
766 *Institution of Civil Engineers-Transport*, 156 (2), 73–83.

767 Leng, Z., et al., 2009. Interface Bonding between Hot-Mix Asphalt and various Portland Cement Concrete
768 Surfaces: Assessment of Accelerated Pavement Testing and Measurement of Interface Strain.
769 *Transportation Research Record*, 2127 (1), 20–28.

770 Liu, J., et al., 2017. Prediction models of mixtures' dynamic modulus using gene expression
771 programming. *International Journal of Pavement Engineering*, 18 (11), 971–980.

772 Mohammad, L.N., et al., 2009. Evaluation of bond strength of tack coat materials in field: Development of
773 pull-off test device and methodology. *Transportation Research Record*, (2126), 1–11.

774 Mohammad, L.N., Raqib, M.A., and Huang, B., 2002. Influence of asphalt tack coat materials on interface
775 shear strength. *Transportation Research Record*, (1789), 56–65.

776 Mrzygłód, B., et al., 2020. Sensitivity analysis of the artificial neural networks in a system for durability
777 prediction of forging tools to forgings made of C45 steel. The international journal of advanced
778 manufacturing technology, 109 (5–6), 1385–1395.

779 Nian, T., et al., 2022. Method to predict the interlayer shear strength of asphalt pavement based on
780 improved back propagation neural network. *Construction and Building Materials*, 351.

781 Ozturk, H.I., and Kutay, M.E.,2014. An artificial neural network model for virtual Superpave asphalt
782 mixture design. International Journal of Pavement Engineering, 15 (2), 151–162.

783 Partl, M.N., et al., 2008. Characterization of Water Sensitivity of Asphalt Mixtures with Coaxial Shear
784 Test. *Road Materials and Pavement Design*, 9 (2), 247–270.

785 Raab, C., et al., 2015. The influence of age on interlayer shear properties. *International Journal of*
786 *Pavement Engineering*, 16 (6), 559–569.

787 Raab, C., El Halim, A.E.H.O.A., and Partl, M.N., 2013. Utilisation of artificial neural network for the
788 analysis of interlayer shear properties. *Baltic Journal of Road and Bridge Engineering*, 8 (2), 107–116.

789 Raab, C., Partl, M.N., and El Halim, A.E.H.O.A., 2009. Evaluation of interlayer shear bond devices for
790 asphalt pavements. *Baltic Journal of Road and Bridge Engineering*, 4 (4), 186–195.

791 Ragni, D., et al., 2020. Analysis of shear-torque fatigue test for bituminous pavement interlayers.
792 *Construction and Building Materials*, 254.

793 Ragni, D., et al., 2022. Investigation into fatigue life of interface bond between asphalt concrete layers.
794 *International Journal of Pavement Engineering*, 23 (10), 3371–3385.

795 Rahman, A., et al., 2017. State-of-the-art review of interface bond testing devices for pavement layers:
796 toward the standardization procedure. *Journal of Adhesion Science and Technology*.

797 Rahman, A., Huang, H., and Ai, C., 2021. Effect of Shear Stresses on Asphalt Pavement Performance and
798 Evaluating Debonding Potential under Repeated Loading: Numerical Study. *Journal of Transportation*
799 *Engineering, Part B: Pavements*, 147 (3).

800 Rahman, A., et al., 2019. Fatigue performance of interface bonding between asphalt pavement layers
801 using four-point shear test set-up. *International Journal of Fatigue*, 121, 181–190.

802 Raposeiras, A.C., et al., 2013. Test methods and influential factors for analysis of bonding between
803 bituminous pavement layers. *Construction and Building Materials*.

804 Roffe, J.C. and Chaignon, F., 2002. Characterisation Tests on Bond Coats: Worldwide Study, Impact,
805 Tests, Recommendations. *In*: *In Proceedings of the 3rd International Conference on Bituminous*
806 *Mixtures and Pavements*. Thessaloniki, Greece,.

807 Romanoschi, S.A. and Metcalf, J.B., 2001. Characterization of Asphalt Concrete Layer Interfaces.
808 *Transportation Research Record*, 1778 (1), 132–139.

809 Salinas, A., et al., 2013. Interface layer tack coat optimization. *Transportation Research Record*, (2372),
810 53–60.

811 Seitllari, A., and Kutay, M.E., 2023. Investigation of the fatigue life relationship among different
812 geometry combinations of the 3-point bending cylinder (3PBC) fatigue test for asphalt concrete.
813 *International Journal of Pavement Engineering,* 24(1), 2159402.

814 Song, W., et al., 2016. Laboratory investigation of interlayer shear fatigue performance between open-
815 graded friction course and underlying layer. *Construction and Building Materials*, 115, 381–389.

Tashman, L., Director, W., and Papagiannakis, T., 2006. *Evaluation of the Influence of Tack Coat Construction Factors on the Bond Strength Between Pavement Layers*. Washington Center for Bituminous Technology, Report No. WCAT 06-002.

Tenpe, A. R., and Patel, A., 2020. Application of genetic expression programming and artificial neural network for prediction of CBR. *Road materials and pavement design*, 21(5), 1183-1200.

Tozzo, C., Fiore, N., and D'Andrea, A., 2014. Dynamic shear tests for the evaluation of the effect of the normal load on the interface fatigue resistance. *Construction and Building Materials*, 61, 200–205.

Uzan J, Livneh M, and Eshed Y., 1978. Investigation of Adhesion Properties between Asphaltic-Concrete Layers. *In*: *In Association of Asphalt Paving Technologists Proc*.

Wang, X., et al., 2017. Shear fatigue between asphalt pavement layers and its application in design. *Construction and Building Materials*, 135, 297–305.

West, R.C., Zhang, J., and Moore, J., 2005. Evaluation of bond strength between pavement layers. No. NCAT Report 05-08. Auburn University. National Center for Asphalt Technology,

Yao, Kang, et al 2024. Influence of bonding condition of different interfaces on the mechanical responses and failure mode of asphalt pavement. *Canadian Journal of Civil Engineering*, 2024.